https://doi.org/10.5194/egusphere-2026-413
Preprint. Discussion started: 23 February 2026


# Co-occurrence of gravity waves, vertical wind shear and turbulence in the lowermost stratosphere over the North Atlantic

Madhuri Umbarkar[1], Daniel Kunkel[1], and Ulrich Achatz[2]

[1]Institute for Atmospheric Physics, Johannes Gutenberg University Mainz, Germany
[2]Institute for Atmospheric and Environmental Sciences, Goethe University Frankfurt am Main, Germany

**Correspondence:** Madhuri Umbarkar (mumbarka@uni-mainz.de) and Daniel Kunkel (dkunkel@uni-mainz.de)

**Abstract.** This study focuses on the spatial and temporal co-occurrence of gravity waves (GW) and of vertical shear and turbulence in the extratropical lowermost stratosphere (LMS). For this, one year of ERA5 reanalysis data is used to analyse the occurrence and variability of resolved GW momentum fluxes, vertical shear, and turbulence indices in the region of the North Atlantic. In the tropopause region GWs can lead to strong vertical wind shear and ultimately to the generation of turbulence, which may result in troposphere-stratosphere exchange and mixing and is a risk for commercial aviation. The occurrences of GWs, shear, and turbulence are analysed in terms of vertical, geographical, and seasonal occurrence frequency distribution and put in relation to the large-scale circulation and to processes related to GW appearances. The contribution of resolved GWs to shear is found to be notable, especially in the North Atlantic winter lowermost stratosphere, where vertical momentum flux convergence provides a peak zonal GW forcing up to -2 $\mathrm{ms}^{-1}\,\mathrm{day}^{-1}$ around 45° N at tropopause altitudes. The prominent vertical propagation in the wintertime mid-latitudes substantially leads to the formation of belt-like structures of GW activity, as evident by momentum fluxes, and further contributes to the pronounced occurrence of shear in the LMS. Ultimately, this study discusses the role of small-scale dynamics in shaping a quasi-permanent layer of elevated shear above the extratropical tropopause and its potential to generate turbulence in this region.

## 1 Introduction

Atmospheric gravity waves (GWs) manifest themselves in the flow as oscillations in a stably stratified atmosphere, which occur as a result of the restoring force of gravity when air is displaced from equilibrium. It is generally accepted that these GWs produce global effects on the atmospheric circulation from the surface up to mesosphere and lower thermosphere region (Fritts and Alexander, 2003; Alexander et al., 2010; Chen et al., 2019). Momentum deposition by vertically propagating GWs to large-scale flow is one of the main physical processes affecting the middle atmosphere circulation (Lindzen, 1981). Originating from the disturbances in balanced flows within stratified environments, e.g., flow over topography, convection, flow instabilities and wave turbulence, they can propagate over large distance, transfer energy, induce turbulence and modify the mean flow dynamics far from their source region (Fritts and Alexander, 2003; Alexander et al., 2010; Sutherland et al., 2019; Achatz et al., 2024).

https://doi.org/10.5194/egusphere-2026-413
Preprint. Discussion started: 23 February 2026


In the extratropical troposphere, GWs arise mainly from orographic and convective sources as well as from jet imbalances. As GWs propagate upward through stratosphere and reaching all the way up to mesosphere, they transport energy and momentum, and deposit them locally in the regions where wave breaking or dissipation occurs. This process, referred to as the GW forcing, plays a key role in the global circulation. However, most of the climate models need to parameterize this process, since they struggle to explicitly resolve the smaller-scale GWs, typically those with horizontal wavelengths shorter than a few hundred kilometers (e.g. Kim et al., 2003; Geller et al., 2013). On both hemispheres, the baroclinic zones in the mid-latitudes and as such the meridional temperature gradient on planetary scales is associated to the jet streams in the upper troposphere and as such to regions of enhanced vertical wind shear at the edges of strong wind systems. Aloft, these westerlies give rise to the jet streams at mid-latitudes, with maximum wind speeds typically occurring near the tropopause, where the sign of meridional temperature gradient reverses. These jets, often referred to as eddy-driven due to their link with sustaining surface westerlies, differ from the subtropical jets. The eddy-driven jets play a central role in shaping mid-latitude storm tracks and have practical implications for aviation, not only by producing strong headwinds and tailwinds along major flight routes but also by generating clear-air turbulence through pronounced vertical shear.

In recent years, there has been growing interest in understanding the role of small-scale GWs in stratosphere–troposphere exchange and mixing within the upper troposphere and lower stratosphere (UTLS) (e.g., Luderer et al., 2007; Kunkel et al., 2019; Gisinger et al., 2020; Lachnitt et al., 2023; Dörnbrack et al., 2025; Umbarkar and Kunkel, 2025; Umbarkar et al., 2025). The UTLS, characterized by strong wind shear, horizontal temperature gradients, and sharp changes in stability, provides both a source and sink for GWs. These conditions influence GW propagation, amplification, and dissipation, with regions of baroclinic instability and jet streaks acting as hotspots for GW generation and interaction with the large-scale circulation (Plougonven and Snyder, 2005; Zhang et al., 2015).

From a model perspective, GWs still pose an open issue, since the models commonly have too coarse resolution to explicitly simulate GWs on the mesoscale and below. Thus, the effect of unresolved GWs on the large-scale circulation remains to be parameterized, if they are to be included (e.g., Kim et al., 2003; Jewtoukoff et al., 2015). Another recent study from Banerjee et al. (2025) hint that both oblique GW propagation and GW-turbulence interactions play an important role in transport and mixing processes in the middle atmosphere and it should therefore be accounted for subgrid-scale parameterizations, although further observational constraints are still needed. Current state-of-the-art reanalysis data, especially the ERA5 reanalysis offer relatively fine temporal and spatial resolution, and resolve central features of the GW spectrum, despite the issues discussed before (e.g., Podglajen et al., 2020; Kaluza et al., 2021; Gupta et al., 2024). ERA5 is able to resolve GWs with wavelengths of a few hundred kilometers and longer (Gupta et al., 2024), thereby contributing to its ability to simulate large- as well as small-scale wave dynamics.

The tropopause wind shear layer (TSL) is recurring and well-developed feature over the North Atlantic (NA) with notably high shear occurrences during boreal winter season as described in Kaluza et al. (2021). Here, we want to study the annual variation of this TSL over the NA and look for the sources of vertical shear, with a particular focus on the role of GWs in the shear enhancement above the local tropopause. The NA is chosen because it exhibits high shear occurrence spanning over the storm track regions (Shaw et al., 2016), and also features different localized meteorological mechanisms that generate

https://doi.org/10.5194/egusphere-2026-413
Preprint. Discussion started: 23 February 2026


GWs in different sectors (e.g., convective and orographic sources of GWs in and over the (eastern) part of North America and (western) Spain). One year has been arbitrary chosen, but as noted in Kaluza et al. (2021), 2017 is one of the years with the most pronounced shear occurrences over the NA in their dataset. We focus not on the long-term trend but on the annual variability and how it relates to the occurrence of GWs.

The interest in strong vertical shear is that it can be a source of turbulent motions. Turbulence can be generated through wave breaking at critical levels where the background wind speed approaches the horizontal phase velocity of propagating GWs (Drnbrack et al., 1995). On one side, turbulent motions foster irreversible mixing of air masses, thus altering the chemical composition of the layer where it occurs. In particular, mixing plays a crucial role in shaping the extratropical transition layer (e.g., Hoor et al., 2004; Hegglin et al., 2009; Pan et al., 2006), which is essentially a layer around the local extratropical tropopause in which the chemical composition is strongly affected by tropospheric and stratospheric dynamics. On the other side, turbulent motions in the extratropical tropopause region can substantially affect air traffic (Kim and Chun, 2011; Sharman and Pearson, 2017; Gultepe et al., 2019). In the future, air traffic might even be more affected by severe (clear-air) turbulence (CAT, de Medeiros and Williams, 2025). For better predictions a more concise analysis of the potential processes leading to turbulence are required. Thus, in this study we explore the spatial and temporal co-occurrences of GWs, vertical shear and potential turbulence over the North Atlantic.

Specifically, we want to address the question whether there are relations in annual cycle of GW, shear, and turbulence occurrences and variability over the North Atlantic in the lowermost stratosphere. Here, in particular focus is on the shape of the TSL and the dynamics behind these potential relations. In the present study, we describe the intra-annual variability of small-scale GW-induced shear over the NA and their representation with the resolution compared to ERA5. We present a step-by-step analysis with justification and limitations for each stage. This paper is organized as follows: after the data and procedure discussed in Sect. 2, the results are discussed in two sections concerning quasi-climatological characteristics of TSL including turbulence indices (Sect. 3), and seasonal to intra-monthly variability of GW resolved fluxes and vertical shear (Sect. 4). Thereafter, the major outcomes are summarized in Sect. 5.

## 2 Data and procedure

The ERA5 reanalysis, developed by the European Center for Medium-Range Weather Forecasts (ECMWF), provides hourly global fields of atmospheric, land-surface, and ocean-wave parameters with high spatial and temporal resolution (Hersbach et al., 2020). Its horizontal grid spacing of $0.25°$, corresponding to $\sim$31 km in latitude/longitude, enables the resolution of GWs with horizontal wavelengths as short as $\sim$100 km (Wright and Hindley, 2018; Gupta et al., 2024). ERA5 also features a fine vertical resolution, with 137 model levels extending up to 0.01 hPa, making it particularly adept to capture GWs with vertical wavelengths down to $\sim$1–2 km. To reduce spurious wave reflections and improve numerical stability, ERA5 incorporates advanced model treatments such as sponge layers and hyper diffusion.

The analysis is based on daily ERA5 reanalysis data in the NA region (35° N–60° N, 60° W–0° W; blue box in Fig. 1) over the annual cycle from March 2017 to February 2018. For our analysis, we use ECMWF data at night (00:00 UTC) but

https://doi.org/10.5194/egusphere-2026-413
Preprint. Discussion started: 23 February 2026


more frequent time-steps (say every 6 hours) are also possible. This daily resolution is sufficient to determine whether the annual cycle of GW momentum fluxes and shear as well as turbulence occurrences are correlated. However, a finer temporal resolution would be required for case-study analysis. In the UTLS between 5–20 km altitude, the grid spacing of vertical levels is about 300–400 m. Below the grid spacing is slightly finer and becomes coarser with altitude. We use basic quantities such as temperature (T) and the three dimensional wind ($u$, $v$, $w$) as well as derived quantities such as potential vorticity (PV) $Q$:

$$Q = \frac{1}{\rho}\boldsymbol{\eta} \times \boldsymbol{\nabla}\Theta, \tag{1}$$

where $\rho$ is the density of the medium, $\Theta$ is potential temperature, the vector of the absolute vorticity $\boldsymbol{\eta} = \boldsymbol{\nabla} \times \boldsymbol{u} + 2\boldsymbol{\Omega}$ which is composed of the rotation of the three dimensional wind field $\boldsymbol{u} = (u, v, w)$, with $u$, $v$ and $w$ the components of the three dimensional wind, and the angular velocity of the earth $\boldsymbol{\Omega}$. The unit for PV is PVU where 1 PVU = $10^{-6}\,\mathrm{m^2\,s^{-1}\,K\,kg^{-1}}$. More so, in this study we use PV to define the extratropical tropopause as the 3.5 PVU isosurface.

The vertical wind shear is defined on the native vertical hybrid sigma-pressure levels of the IFS to retain the maximum amount of information in the gradient base measure. The altitude at each model level is derived from the geopotential after vertically integrating the hydrostatic equation from the pressure, temperature and specific humidity profiles. The vertical shear is then derived using the zonal ($u$) and meridional ($v$) wind components:

$$S^2 = \left(\frac{\partial u}{\partial z}\right)^2 + \left(\frac{\partial v}{\partial z}\right)^2. \tag{2}$$

It should be taken into consideration that the increasing vertical grid spacing with increasing altitude in the native coordinates may result in a potential bias towards larger values of vertical wind shear at lower altitudes. However, in the UTLS region, the vertical grid spacing increases from around 300 m at 5 km altitude up to around 400 m at 20 km altitude (e.g., Hoffmann et al., 2019). Thus, the resolution bias unlikely contributes substantially to the results here.

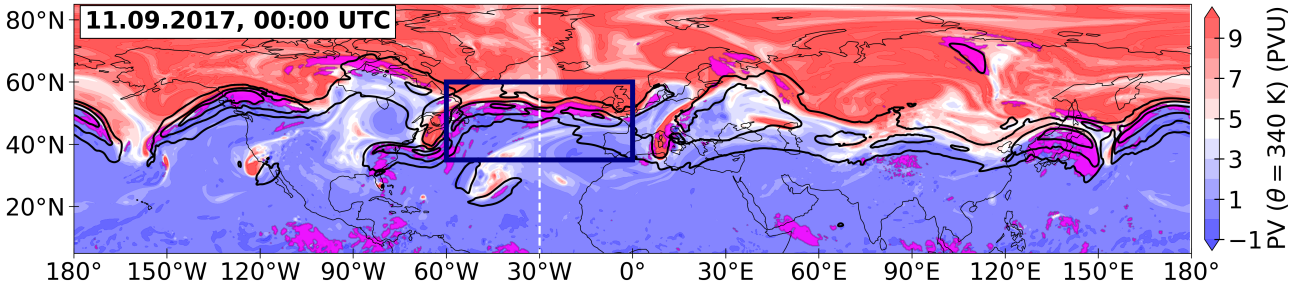


**Figure 1.** Snapshot of potential vorticity at 340 K isentropic surface over the northern hemisphere on 11 September 2017, 00:00 UTC. The solid black lines represents the horizontal wind beginning at 30 m $\mathrm{s^{-1}}$ in steps of 15 m $\mathrm{s^{-1}}$ at 200 hPa pressure surface. Magenta shaded areas represent regions of $S^2 \geq S_t^2$ where $S_t^2 = 4 \times 10^{-4}\,\mathrm{s^{-2}}$, between 3.5 PVU dynamical tropopause and 1.5 km above. Dashed vertical lin indicates the location of vertical cross section shown in Fig. 9. The blue box indicate the North Atlantic domain selected for this study that features a characteristic sequence of wave-like patterns and strong shear maxima in the vicinity of upper tropospheric jet region.

https://doi.org/10.5194/egusphere-2026-413
Preprint. Discussion started: 23 February 2026


Figure 1 presents a snapshot of the northern hemispheric PV distribution on the 340 K isentropic surface for 11 September 2017, 00:00 UTC, and maxima of the horizontal wind at 200 hPa. A distinct feature is the pronounced tropopause break and its close link to jet streaks in the upper-level flow. Over the Asian continent extending into the western Pacific, the PV structure exhibits a sharp meridional gradient that coincides with a coherent subtropical jet. Toward the western sector, the PV gradient becomes weaker and organizes into a sequence of Rossby or gravity wave like patterns generated via baroclinic flow and each associated with jet streaks occurring at different latitudes.

The momentum transport due to small-scale is investigated via: (i) the absolute momentum flux which includes the zonal ($\rho\overline{u'w'}$) and meridional ($\rho\overline{v'w'}$) flux components, and (ii) the vertical momentum flux convergence ($-\frac{\partial}{\partial z}\overline{u'w'}$; hereafter VMFC) term from the Eliassen-Palm flux divergence. The derivation of perturbation quantities is described in Appendix A. The latter represents the net forcing of the mean flow by resolved wave fluxes due to GWs (e.g., Fritts and Alexander, 2003). We use this term to assess both vertical and meridional transport of resolved GW momentum fluxes contributing to the forcing of the zonal flow and to estimate the associated wave-induced forcing. The fluctuations of short-scales from the large-scale background flow are referred to the small-scale perturbations induced by GWs (hereafter GW perturbations). Note that, the momentum flux of the sub-synoptic scales is treated here as a quasi-proxy for momentum flux due to GWs. We summarize briefly how the GW proxies are calculated in the following paragraph.

The GW perturbations from synoptic-scale structures are quantified using a hybrid method (similar to Wei et al., 2022; Umbarkar and Kunkel, 2025; Umbarkar et al., 2025). The selection of this hybrid approach is motivated by its ability to effectively capture the patterns of small-scale GWs (Zhang et al., 2025). This selection criterion is based on both the scale and structural characteristics of the perturbations. The frequency and wavelength of these perturbations are also critical identifiers of GW scales, distinguishing them from other atmospheric phenomena. As part of processes understanding, we focus particularly on small-scale GWs, excluding any with wavenumber $\leq 20$ and considering the covariance only from zonal wavenumbers 21 and higher, following Gupta et al. (2021, 2024). See Appendix A for detailed description. The absolute momentum flux (MF) is then computed from perturbation fields as follows:

$$\mathrm{MF} = \rho\sqrt{(\overline{u'w'})^2 + (\overline{v'w'})^2}, \tag{3}$$

where $\rho$ is the mean density, and $u'$, $v'$, $w'$ is the vector of wind perturbations. Note that MF values are shown as a base-10 logarithm of flux magnitude throughout the analysis.

The shear perturbations calculated using perturbation quantities to solely investigate the GW-induced shear (from now on referred as $S^{2'}$). Furthermore, the tropopause shear layer existence is identified by $S^2 \geq S_t^2$ following Kaluza et al. (2021) based on the occurrence frequency of such shear exceeding a defined threshold, where $S_t^2 = 4 \times 10^{-4}\,\mathrm{s}^{-2}$, in the tropopause-based coordinate system for the selected year over the North Atlantic.

To further capture both the dynamical and kinematic aspects of turbulence generation in the UTLS affected by GWs, we identify the potential turbulence regions via: i) the gradient Richardson number $Ri$ and ii) the Ellord turbulence indices, TI1 and TI2. According to linear theory, the dynamic stability of a fluid within stratified shear flow can be identified using $Ri$ and

https://doi.org/10.5194/egusphere-2026-413
Preprint. Discussion started: 23 February 2026


can be written as:

$$Ri = \frac{N^2}{S^2} = \frac{\frac{g}{\theta}\cdot\frac{\partial\theta}{\partial z}}{\left(\frac{\partial u}{\partial z}\right)^2 + \left(\frac{\partial v}{\partial z}\right)^2} \tag{4}$$

where $N^2$ is the squared Brunt-Vaisälä frequency, also known as static stability, and $g$ denotes the acceleration due to gravity at the Earth's surface.

Following Ellrod and Knapp (1992); Sharman et al. (2006), the turbulence indices TI1 and TI2 and their constituents are computed on the smaller-scales as outlined in Umbarkar et al. (2025). The TI1 is calculated using vertical shear perturbations and flow deformation (DEF) as:

$$\mathrm{TI1} = S' \times \mathrm{DEF} = \left(\left(\frac{\partial u'}{\partial z}\right)^2 + \left(\frac{\partial v'}{\partial z}\right)^2\right)^{1/2} \times \left(\left(\frac{\partial u'}{\partial x} - \frac{\partial v'}{\partial y}\right)^2 + \left(\frac{\partial v'}{\partial x} + \frac{\partial u'}{\partial y}\right)^2\right)^{1/2}. \tag{5}$$

TI2 which additionally considers flow convergence (CVG) related to the development of upper-level frontal zones, thereby strengthens vertical wind shear, is derived using;

$$\mathrm{TI2} = S' \times (\mathrm{DEF}+\mathrm{CVG}) = \left(\left(\frac{\partial u'}{\partial z}\right)^2 + \left(\frac{\partial v'}{\partial z}\right)^2\right)^{1/2} \times \left[\left(\left(\frac{\partial u'}{\partial x} - \frac{\partial v'}{\partial y}\right)^2 + \left(\frac{\partial v'}{\partial x} + \frac{\partial u'}{\partial y}\right)^2\right)^{1/2} - \left(\frac{\partial u'}{\partial x} + \frac{\partial v'}{\partial y}\right)\right]. \tag{6}$$

Note that TI1 and TI2 presented here are derived from the perturbation wind components ($u'$, $v'$), and thus are based mainly on the GW-scale features.

## 3 Annual cycle of strong vertical wind shear and turbulence indices in the UTLS over the North Atlantic

### 3.1 Vertical distribution and intra-monthly variability of strong vertical wind shear

We will start with an analysis of the intra-annual variability of occurrences of TSL over the course of one year of daily ERA5 fields. For this, we follow the analysis steps outlined in Kaluza et al. (2021) and start with a presentation of vertical distribution of strong vertical wind shear $S^2 \geq S_t^2$, followed by an examination of its geographic occurrence frequency distribution across the NA lowermost stratosphere.

We proceed with the analysis of monthly vertical distribution of strong vertical wind shear which is defined by an exceedance of a threshold value. Figure 2 shows the zonal average occurrence frequency for $S^2 \geq S_t^2$. In the vertical, the occurrence distributions are transformed into a tropopause following coordinate system with the dynamical tropopause, i.e., $Q = 3.5\,\mathrm{PVU}$ isosurface, as reference altitude (see e.g., Birner, 2006; Kaluza et al., 2021). Following Kaluza et al. (2021) we refer to the region above the tropopause with the maximum values in the occurrence frequency as the tropopause shear layer (TSL). The annual cycle of the TSL reveals a year round presence of the TSL between 35–60° N and between the level of the tropopause and roughly two kilometers above. While the extent varies more in the vertical with a deeper TSL in winter/early spring and a more shallow appearance during summer, the meridional extent shows only minor variations over the course of the year. Only in late summer (July through September) the region of maximum occurrence frequencies has a slightly smaller meridional extent

https://doi.org/10.5194/egusphere-2026-413
Preprint. Discussion started: 23 February 2026


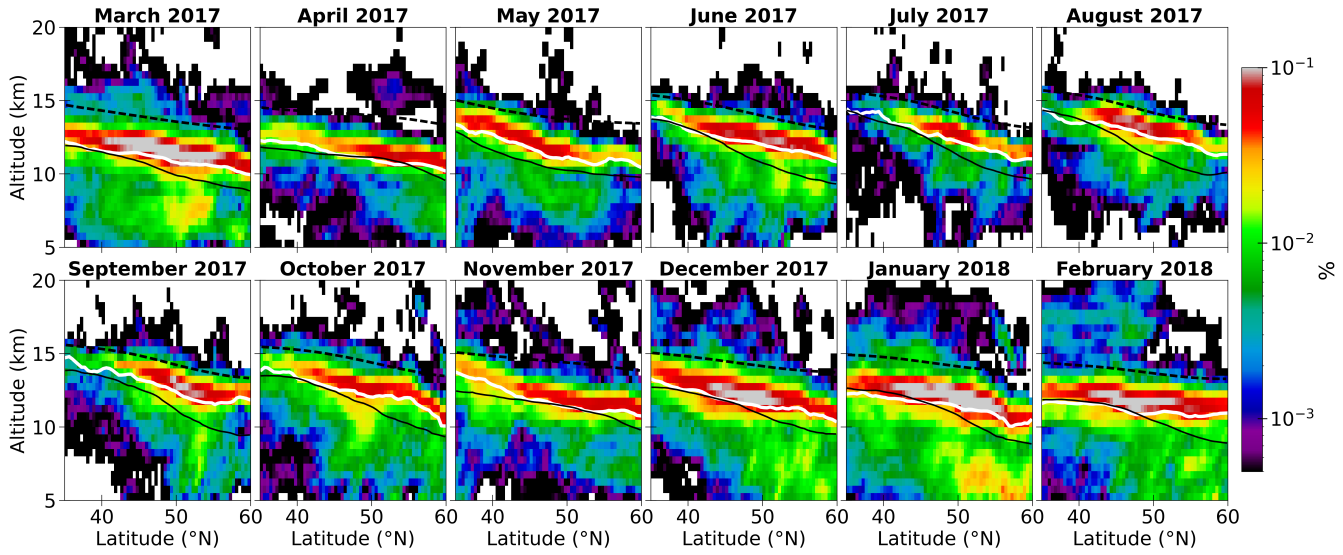


**Figure 2.** Occurrence frequency distribution of $S^2 \geq S_t^2$ with tropopause-based vertical coordinate system from March 2017 to February 2018. The mean dynamical tropopause altitude for profiles $S^2 \geq S_t^2$ restored (from mean tropopause altitude + dz from the tropopause altitude) shown as white line. The occurrence frequencies are shown with logarithmic frequency contours, displaying the data in bins of sizes $\Delta y = 0.4°$ and $\Delta z = 500$ m. The zonal-mean dynamical tropopause (3.5 PVU isosurface; black solid line) and the zonal-mean 380 K isentrope of potential temperature (black dashed line) are overlaid.

and the maximum occurrences are slightly shifted polewards compared to other months. The absolute occurrence frequencies show a more obvious annual cycle with maximum occurrences in winter and early spring with maximum values on the order of 1–10 %. This occurrence frequency follows largely the strength and location of the eddy driven jet in the extratropics.

This finding supports the fact that large-scale dynamics play an important role. Although the clustering of $S^2 \geq S_t^2$ agrees with the dynamic stability criterion, as well as the thermal wind associated with the baroclinicity at upper-tropospheric fronts, the significance of processes related to the occurrence of the TSL still remains to be quantified. Related to that, we now discuss the influence of large-scale jet dynamics on the intensity of TSL (Fig. 3), before moving on to the role of small-scale processes.

**Mean meteorological state over the North Atlantic**

Figure 3 shows the monthly mean zonal wind and horizontal wind together with the regions of strong shear between the dynamical tropopause and 1.5 km above over the NA. The jet stream reaches its maximum strength in winter (December-January), with wind speed exceeding 50 $\mathrm{m\,s^{-1}}$. During these months, the jet axis is displaced farthest south, typically located between 35–45° N over western and central NA. In contrast, from June to August the jet structure weakens and shifts northward, with the core positioned around 45–55° N. The seasonal displacement is accompanied by a intensity of meridional baroclinicity and upper-level jet stream strength.

https://doi.org/10.5194/egusphere-2026-413
Preprint. Discussion started: 23 February 2026


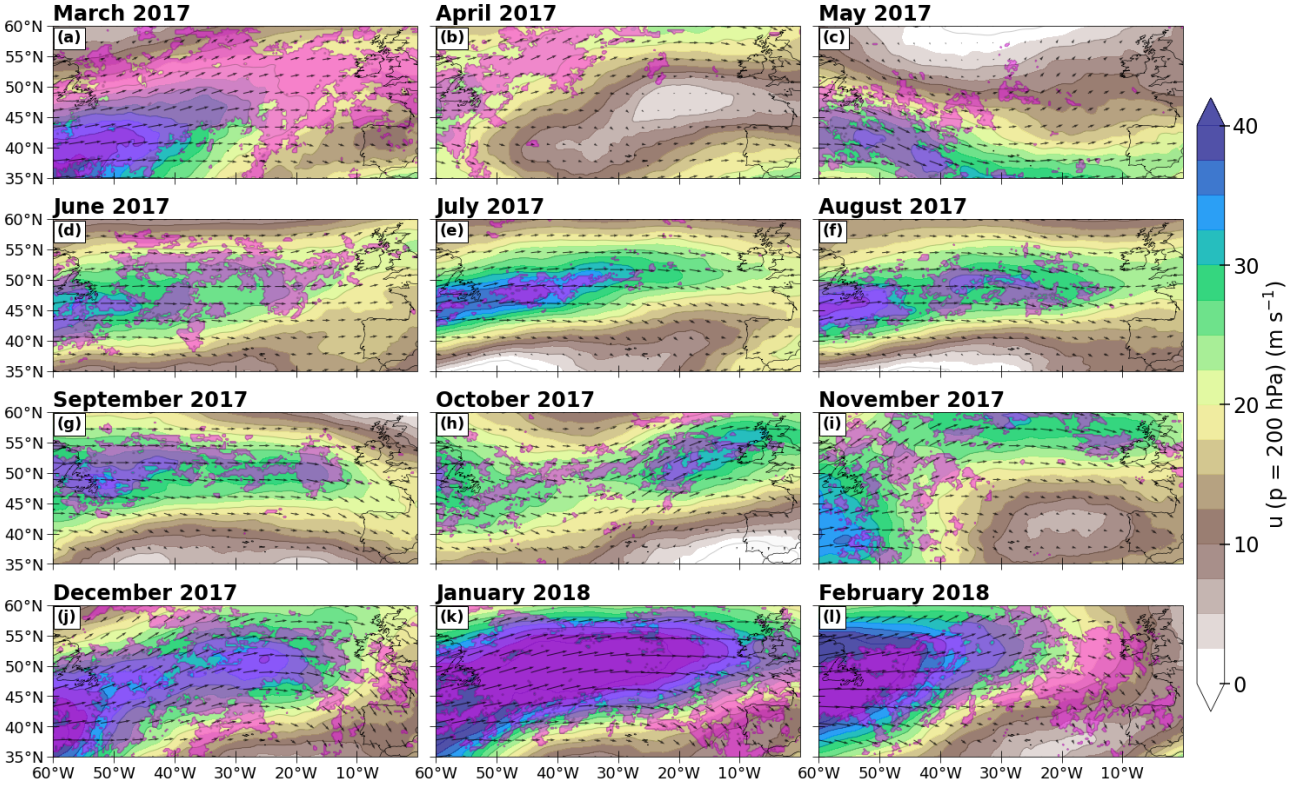


**Figure 3.** The 200 hPa monthly mean zonal wind (shaded; $\mathrm{m\,s^{-1}}$) and horizontal wind vectors (arrows) over the North Atlantic from March 2017 to February 2018. Magenta shaded areas represent the occurrences of strong vertical wind shear $S^2 \geq S_t^2$ where at least once the threshold is exceeded between 3.5 PVU dynamical tropopause and 1.5 km above in the respective month.

Throughout the year, a clear coherent band of strong wind shear (magenta) is apparent mainly near the jet core, where each region can be attributed to a planetary circulation feature (see Kaluza et al., 2021, for discussion). This band also migrates meridionally with the jet: southward and more intense in winter and early spring, and weaker and positioned farther north in the summer. The pronounced shear occurs along the climatological storm track regions (Shaw et al., 2016), where shear maxima extend zonally from eastern North America across central NA into western Europe. In addition to this large-scale jet related shear structure, several small-scale shear patches appear sporadically and can be associated with transient synoptic systems such as extratropical cyclones, warm conveyor belts, stratospheric cut-offs, and localized GW activity embedded within the baroclinic flow.

Especially during winter, the wind systems described above align closely with the meridional band of frequent occurrences of strong vertical wind shear near the tropopause (Fig. 2). At mid-latitudes, the tropopause region exhibits strong shear within Rossby-wave jet streaks and along the curled-up ridges associated with breaking baroclinic waves (Kaluza et al., 2019, 2021). The latter is frequently exposed to enhanced GW activity and hence, hints at their link to the formation of the TSL due to

https://doi.org/10.5194/egusphere-2026-413
Preprint. Discussion started: 23 February 2026


their bi-directional interaction with the thermal stratification gradients. Therefore, we discuss the relevance of GW-induced momentum fluxes to the observed shear layers in the subsequent analysis (Sect. 3.2).

## Vertical wind shear in the LMS

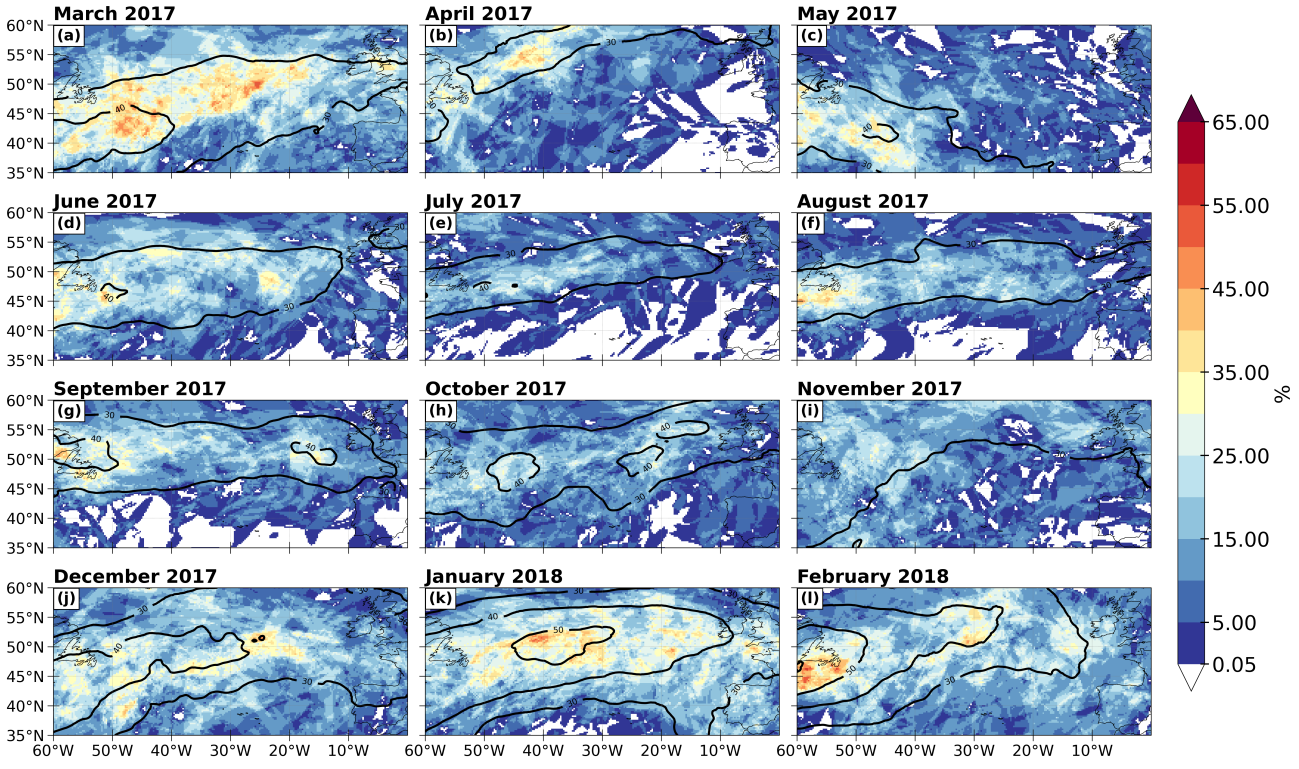


**Figure 4.** Occurrence frequency distributions of $S^2 \geq S_t^2$ in the LMS (i.e., the region between dynamical tropopause and 380 K isentrope) in the North Atlantic from March 2017 to February 2018. The solid black lines represents the horizontal wind beginning at 30 m s$^{-1}$ in steps of 10 m s$^{-1}$ at 11 km altitude.

We now proceed with the analysis of the geographical distribution of the vertical shear $S^2$ exceeding the threshold $S_t^2$ that is located between the dynamical tropopause and 380 K isentropic surface (Fig. 4). For that, we count how often $S^2 \geq S_t^2$ criterion is met at each grid point during all time steps for each month and normalize it by total number of data points per month in each grid box. The resulting distribution reveals a distinct annual cycle of these quasi-horizontal occurrence frequencies of strong shear over the NA lower stratosphere.

From our data, it becomes evident that the NA exhibits several hotspots of high shear encounters (Fig. 4). In particular, we see the most extensive occurrences appear during winter (December–February), where a dominant shear maximum emerges southwest of Ireland and another, more zonally oriented maximum stretches from Newfoundland across the central NA. These regions are in close proximity to the jet-core during the time of the strongest jet in the winter season. In contrast, summer

https://doi.org/10.5194/egusphere-2026-413
Preprint. Discussion started: 23 February 2026


months (Fig. 4b-d) show weaker and more spatially confined shear, consistent with the poleward shift and weakening of the upper tropospheric jet. Autumn (Fig. 4g-i) months display a gradual re-intensification of shear along the jet in association with the increasing baroclinicity.

At mid-latitudes, the high shear occurrences are most pronounced during winter and are associated with jet streaks of the eddy-driven jet, with maxima centered between 40° N-55° N and around 60° W-30° W. Overall, the strong shear exhibits a distinct seasonality over NA. The recurrent occurrence of enhanced vertical shear around the tropopause could be further linked to jet streaks and consequently, to the associated baroclinic wave patterns. Thus, the intra-annual variability of strong vertical shear largely reflects the variability of the jet stream.

### 3.2 Vertical distribution of GW momentum flux

In a next step we want to dive deeper into the annual cycle of gravity wave occurrence in the LMS. We suspect that GW might contribute to the shear in the LMS and particularly that there is a similar annual cycle of GW and shear occurrences in this region.

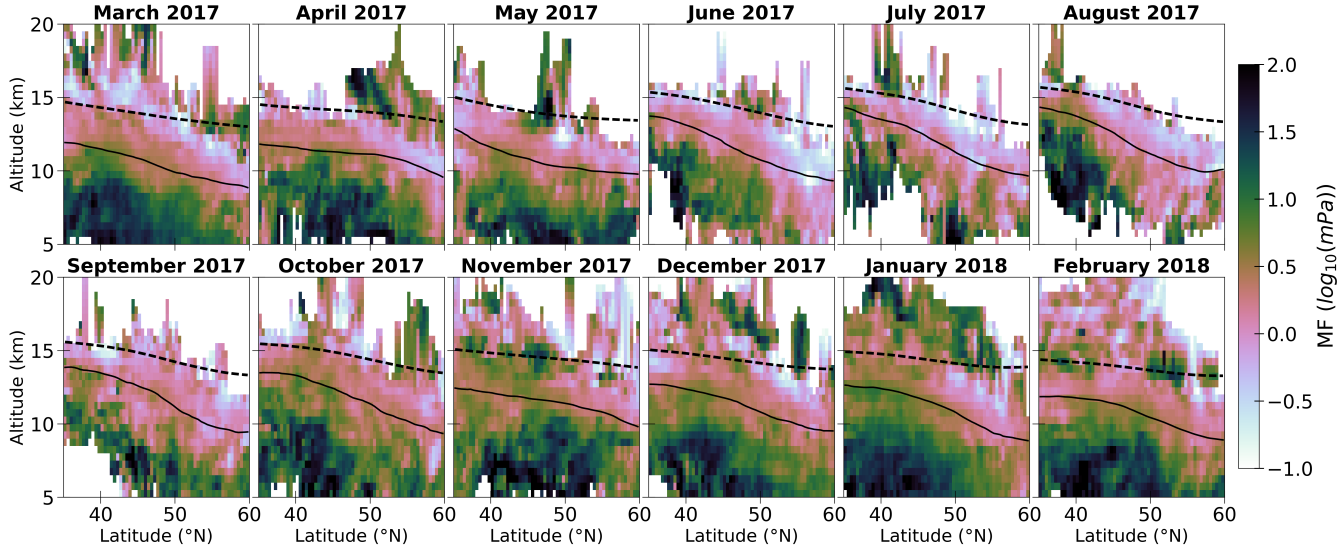


**Figure 5.** Zonal mean of resolved GW absolute momentum flux ($\mathrm{MF}, \log_{10}(\mathrm{mPa})$) values conditioned on regions where $S^2 \geq S_t^2$, i.e., MF in the vicinity of strong shear, from March 2017 to February 2018. The data is shown in bins of sizes $\Delta y = 0.4°$ and $\Delta z = 500$ m. The zonal-mean dynamical tropopause (3.5 PVU isosurface; black solid line) and the zonal-mean 380 K isentrope of potential temperature (black dashed line) are overlaid.

The relation between GWs and TSL is assessed by the tropopause-relative vertical distribution of monthly mean MF in the vicinity of higher occurrences of strong wind shear $S^2 \geq S_t^2$ (Fig. 5). In general, shorter GWs that propagate more vertically carry a larger absolute momentum flux.

https://doi.org/10.5194/egusphere-2026-413
Preprint. Discussion started: 23 February 2026


In the tropopause-based coordinate system, the change in composite GW momentum flux in the vertical coincide with regions of enhanced shear, where the maximum gradients occur below the TSL. In particular, the vertical distribution of MF reveals three prominent features: (i) the upper tropospheric enhanced MF hints at intense upward propagating GW activity (around ∼5–10 km), but could also related to the other small-scale processes such as convection or processes within clouds (e.g., in-cloud dynamics), (ii) the areas of distinct maxima with strong MF abundance in the close vicinity of the tropopause, and (iii) pronounced vertical gradients in the upper branch of lowermost stratosphere. These patterns demonstrate that shear hotspots systematically co-locate with regions of strong GW activity, with substantial MF transport both across the tropopause and within the LMS.

During boreal winter (December–February), the MF exhibits a broader spatial (Fig. B1) and vertical extent, with higher MF values co-occurring in the vicinity of higher $S^2$. Additionally, a sharp vertical gradient of MF upward is evident towards the lower stratosphere. This indicates the pronounced GW activity, especially around 40–50° N near 11–14 km altitude. In contrast, the summer (June–August) features finer small-scale flux structures and stronger vertical gradients throughout the UTLS, likely associated (at least partly) with non-orographic GWs. However, MF magnitudes are substantially reduced and remain confined to lower altitudes, consistent with weaker shear and reduced wave propagation into the lower stratosphere.

Overall, the spatial and seasonal co-location of elevated MF with strong shear suggests a potential role of GWs in the formation of above-tropopause shear layers.

### 3.3 Vertical distribution of turbulence indices

The GWs and in particular their relation to the TSL owe their potential importance to the fact that both features contribute to the formation of the mixing layer around the extratropical tropopause (e.g., Hoor et al., 2004; Pan et al., 2006). If small-scale processes play a role in the formation of the shear layer, their contribution is also expected to be relevant for the generation of (clear-air) turbulence, given that vertical shear is one of the key precursors for turbulence in the UTLS. In addition to that, the strong horizontal deformation has usually been linked to upper-level frontogenesis, may also be an indication of the influence of GWs generated due to flow imbalance (Knox et al., 2008), which could ultimately lead to the development of CAT. Related to that, we move our discussion to the potential occurrence of turbulence due to small-scales in the NA domain. Note that we use large-scale proxies from the resolved variables to study the occurrence of small-scale processes.

Figure 6 presents the extension of previous analysis in the form of occurrence of $0 \leq Ri \leq 1$ in tropopause-based vertical coordinate system, i.e., highlighting regions susceptible to potential dynamic instability. The overall vertical distribution of subcritical $Ri$ occurrences shows that these low Richardson numbers occur most commonly in the upper troposphere during all months. However, the occurrence frequency shows a clear annual cycle: low Richardson numbers are most frequent from November to March while they show lower occurrences during the most other months. Interestingly, there are smaller hotspots of enhanced occurrence frequency during June, August and September which might be related to specific dynamical events. Another interesting feature is that low Richardson number occurrences in the LMS occur more often during winter and as such the potential for turbulence occurrences is enhanced during the winter months compared to the summer months (Kaluza et al., 2022). However, this is no longer the case in the upper part of the lowermost stratosphere. As discussed in Kaluza et al.

https://doi.org/10.5194/egusphere-2026-413
Preprint. Discussion started: 23 February 2026


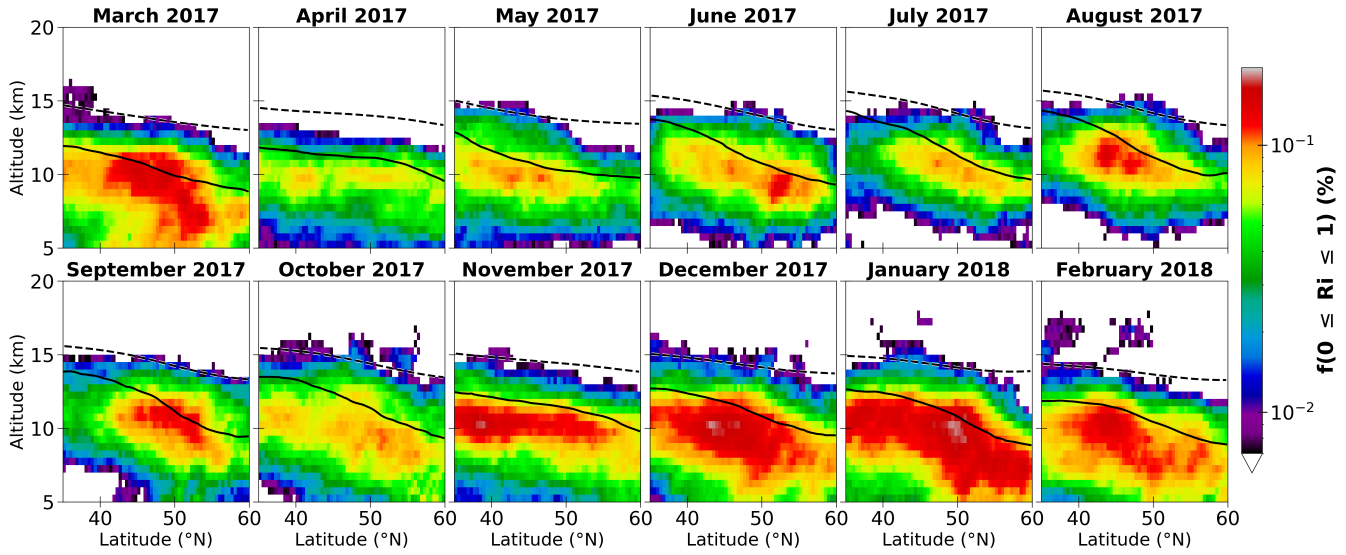


**Figure 6.** Monthly occurrence frequency distribution of $0 \leq Ri \leq 1$ with tropopause-based vertical coordinate system from March 2017 to February 2018. The occurrence frequencies are shown with logarithmic frequency contours, displaying the data in bins of sizes $\Delta y = 0.4°$ and $\Delta z = 500$ m. The zonal-mean dynamical tropopause (3.5 PVU isosurface; black solid line) and the zonal-mean 380 K isentrope of potential temperature (black dashed line) are overlaid.

(2022), this could be related either to model-based $Ri$ values underrepresenting the occurrence of low $Ri$ at subgrid scales, or to a systematic underestimation of vertical shear near the tropopause that stem from the IFS, resulting in rather conservative estimates of the occurrence frequency with regard to shear instabilities in this region (Schäfler et al., 2020). This overall annual pattern of $Ri$ exhibits slightly different vertical distribution from $S^2$ exceedance in the UTLS discussed in Sect. 3.1. This difference likely arises from additional sources causing low $Ri$ other than vertical shear alone, and could therefore be partly associated with GW activity (Sect. 3.2).

To further understand the GWs role to potential turbulence occurrence, we resort to the vertical distribution of empirical turbulence indices (Ellrod and Knapp, 1992) in the following paragraph.

As done for the vertical shear, we also present the occurrence frequency of turbulence diagnostics TI1 and TI2 in a tropopause-based coordinates (see Figures 7 and 8). This has been shown to give a more coherent structure than the view in a surface-based coordinate system (Kaluza et al., 2022).

We start here with occurrences of TI1 exceeding the threshold value, 7 $\times 10^{-7}\,\mathrm{s}^{-1}$ selected based on 95th percentile of the calculated CAT diagnostics (Lee et al., 2020, 2022; Thompson and Schultz, 2021), and we assume that if this threshold is satisfied, moderate intensity turbulence could occur within the given grid cell. Since the spatial and temporal patterns of climatological indices are weakly sensitive to the choice of thresholds, the main focus in the remainder is not on the absolute values of turbulence frequencies, but rather on their spatial patterns. It is important to note that turbulence rarely develops as a single continuous area; instead, it appears in sporadic, short-lived pockets around the periphery of unstable regions (Sharman

https://doi.org/10.5194/egusphere-2026-413
Preprint. Discussion started: 23 February 2026


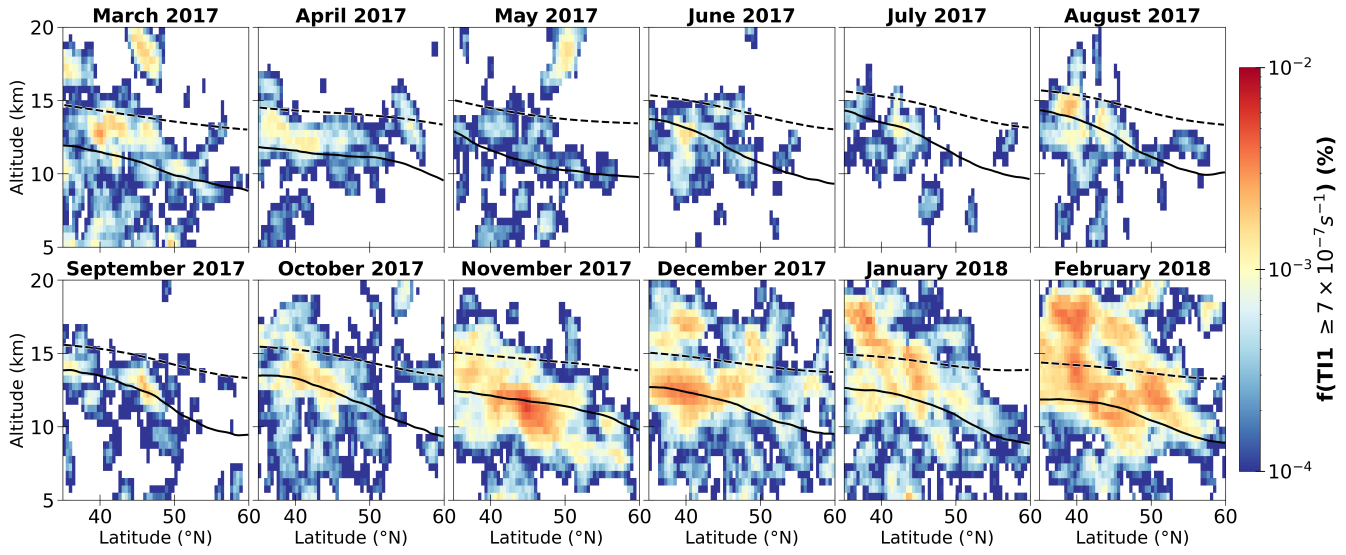


**Figure 7.** Monthly occurrence frequency distribution of TI1 $\geq 7 \times 10^{-7}\,\mathrm{s}^{-1}$ from March 2017 to February 2018. The occurrence frequencies are shown with logarithmic frequency contours, displaying the data in bins of sizes $\Delta y = 0.4°$ and $\Delta z = 500$ m. The zonal-mean dynamical tropopause (3.5 PVU isosurface; black solid line) and the zonal-mean 380 K isentrope of potential temperature (black dashed line) are overlaid.

et al., 2006). Although ERA5 data available at an hourly resolution, the analysis shown here relies on daily single-time-step fields. While the choice may preclude the representation of such short-lived events, the diagnostics are based on relative occurrences that are normalized at each grid box. Thus, the observed structure should be interpreted as an indicator of favorable conditions for their occurrences, rather than a complete census of all short-lived occurrences.

The monthly distributions of TI1 (Fig. 7) indicate that turbulence occurrences cluster in the vicinity of the LMS throughout the year, with enhanced frequencies evident between 40° N and 55° N, broadly following the latitude band of the mid-latitude jet stream. The most pronounced occurrences appear during late autumn and winter (November–February), particularly around 10–13 km altitude, indicating an increased likelihood of small-scale induced turbulence during these months. In contrast, summer (June–August) exhibits substantially reduced TI1 occurrences, consistent with weaker vertical shear and likely related to the reduced GW activity.

It should, however, be noted that neither the Richardson number nor the TI1 are solely defined by $S^2$. On the sub-synoptic scale, the flow deformation, convergence and differential temperature advection can result in frontal zones with the associated wind shear according to the thermal wind relation (Ellrod and Knapp, 1992). In fact, in our analysis, these processes are the major influences of GW activity. In particular, if GWs are involved, they may propagate and perturb the environmental conditions further away from the sources, acting as non-local causes of clear-air turbulence, for instance, when the perturbed regions become unstable and create conditions favorable for Kelvin-Helmholtz instability. We note that this is key for the potential occurrence of clear-air turbulence, as highly transient yet frequent mixing processes in the extratropical lowermost

https://doi.org/10.5194/egusphere-2026-413
Preprint. Discussion started: 23 February 2026


stratosphere. Here, the seasonal pattern suggests that regions of enhanced turbulence activity align closely with the altitudes and latitudes featured by frequent strong shear layers that occur under the influence of GW activity in the LMS.

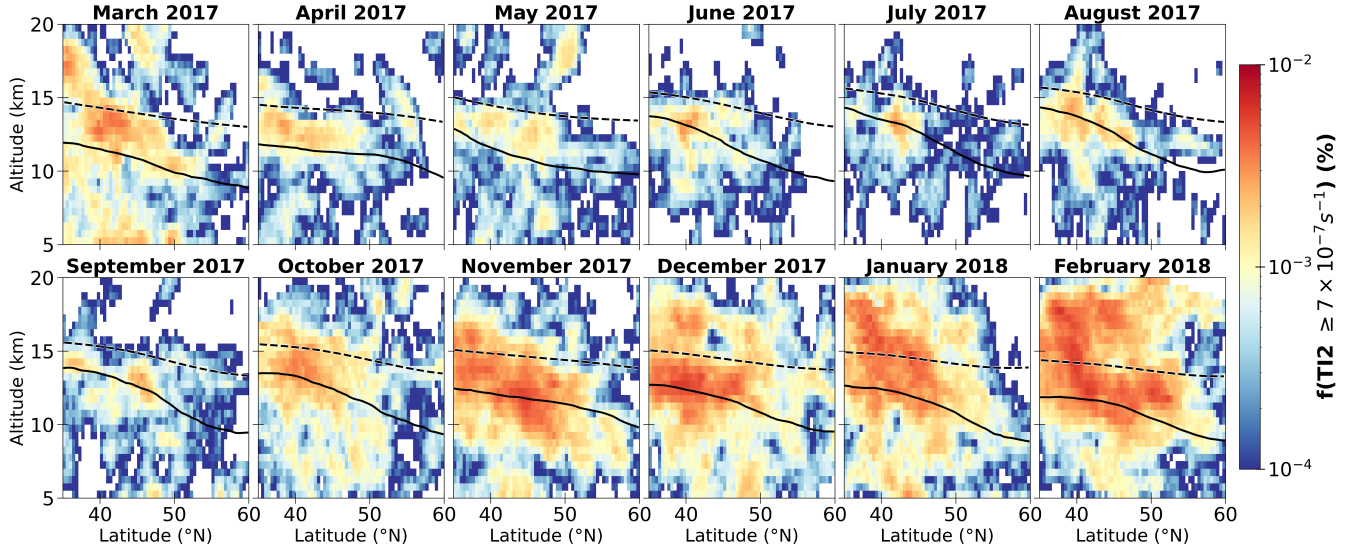


**Figure 8.** Same as Fig. 7 but for TI2.

Besides this, the Ellord-Knapp Turbulent Index (TI1) has been shown to be capable of detecting 70 %–84 % of CAT occurrences (e.g., Ellrod and Knapp, 1992; Sharman and Pearson, 2017; Kim et al., 2018; Gultepe et al., 2019; Thompson and Schultz, 2021). However, the inclusion of the flow convergence term in TI2 offers an advantage over TI1 by capturing the small-scale flow features, such as those associated with GWs or upper-level frontal structures. This gives a more direct relation to GW dynamics in order to understand the relationship between GWs and the development of potential CAT.

The monthly distribution of enhanced TI2 occurrences (Fig. 8) highlight that TI2 maxima are mostly evident in the LMS and are tightly aligned with the tropopause. These regions are also regions that exhibit sharp MF gradients as well as high GW intensity and has a certain resemblance to the annual cycle of the GW discussed in the section before. Thus, this co-location hints at a link between GW-induced small-scale shear and potential turbulence that tend to occur in regions where the tropopause exhibits variations in its fine-scale structure. The elevated wintertime occurrence remains pronounced, but the vertical extent of enhanced TI2 is more sharply confined than TI1, emphasizing that most TI2 events occur within $\pm 2$ km of the tropopause. The occurrence of TI2 maximizes near the tropopause which must be linked to the dynamical and thermodynamical structure of the UTLS. While the overall pattern is similar to that of TI1, TI2 rather shows higher occurrence frequencies and spatial and temporal structures that more closely resemble to $S^2$ and $Ri$.

Moreover, associated with the region of most intense turbulence related shear are the patches of increased high risk CAT occurrences. These intense CAT occurrences show that after some strong shear occur, the moderate intensity CAT occurred at, polewards and upwards the shear layers. In addition, as expected, the GW momentum fluxes consistently exhibit enhanced small-scale vertical gradients in the vicinity of strong shear and turbulence potential (see Sect. 3.2). Overall, the higher vertical

https://doi.org/10.5194/egusphere-2026-413
Preprint. Discussion started: 23 February 2026


gradients of momentum fluxes are evident in the regions where there are pronounced shear and indications of (clear-air) turbulence. Combining all this information suggests the substantial contribution of small-scales, mainly GWs, to the formation of TSL and consequently to hotspots of potential turbulence occurrences.

To conclude, our results demonstrate that there is a quasi-permanent layer of high shear occurrences (that has formerly been framed as the TSL), that has a close resemblance to the annual cycle of the GWs as well as GW-induced CAT potential over the NA. Nevertheless, the question remains whether GWs modulate the formation and maintenance of the extratropical shear layers or are merely a passive response to the background flow variability. This will be further addressed in-depth in Sect. 4.

# 4 Annual variation of GW activity and its potential contribution to shear and turbulence over the North Atlantic lowermost stratosphere

## 4.1 Examples of concurrent GWs and enhanced shear events over the North Atlantic

Before presenting the annual co-variability of GWs and shear, we first present four examples of different GW events, one for each season, over the NA for selected time steps in 2017. These cases shall illustrate the co-location of GWs and shear in the dynamical and thermodynamical environment of the tropopause region.

The synoptic scale horizontal divergence distribution for some GW events at 30° W is shown in Fig. 9a-d. The divergence, used here as a proxy for GW activity, shows undulations in the dynamical tropopause that are indications of upward propagating GWs, with wave amplitudes extending through the lower stratosphere (around 12–17 km). The observed packets of GWs in all cases propagate only a short horizontal distance, while spanning vertically up to ∼17.5 km in altitude, suggesting a low ground-based phase speed and a narrower vertical wavelength. In the case in March, the GW exhibits much finer horizontal structures and larger amplitudes, with a notably shorter vertical wavelength (∼2–3 km, Fig. 9a) evident at 25° N and 45° N. In contrast, in the cases in June and September the GWs show a smaller amplitude with vertical wavelengths of ∼1-2 km. In December, the divergence reveals a more pronounced, vertical propagating wave packet with amplitudes extending higher up into the lower stratosphere and a vertical wavelength of roughly 4–5 km around 45° N (Fig. 9d). Important to note is the close proximity in all cases to the jet stream.

The corresponding vertical distribution of shear (Fig. 9e-h) shows the maximum shear, with values up to $5 \times 10^{-4}\,\mathrm{s}^{-2}$, occurring along the ridges and near the tropopause folds. For all cases, the shear maxima tend to occur close to GWs, typically along the sloping tropopause in the ridge of the baroclinic wave, likely above the lifted air masses that reach the tropopause and beyond, which in turn could affect the shear values there. This spatial overlap implies that GWs locally modulate the background flow and amplify vertical gradients in wind and temperature.

Although the shear in December exhibits a pattern that closely resembles that of March, the spatial extent of shear maxima is notably smaller in the vicinity of the ridge. In June and September, shear values are weaker at 55° N at around 11 km and higher altitudes, but the GWs are also less apparent there. Nonetheless, the strong shear related to the phase of GWs modes remains consistent among all events. Overall, the upward propagating large amplitude GW signals observed in Fig. 9a-d, indicate a spatiotemporal co-location of GWs and vertical wind shear. This holds an important piece of information about the jet

https://doi.org/10.5194/egusphere-2026-413
Preprint. Discussion started: 23 February 2026


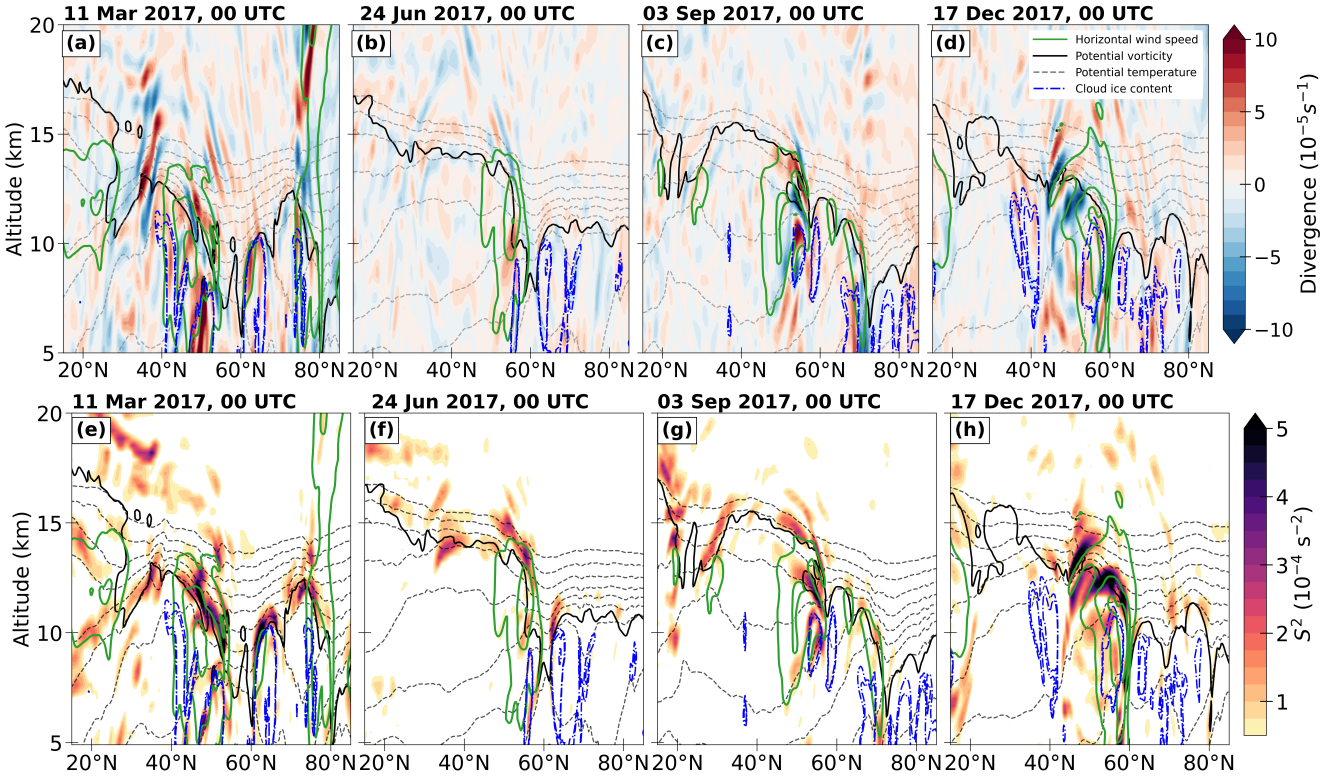


**Figure 9.** Distribution of horizontal divergence at 30° W for (a) 11 March, (b) 23 June, (c) 3 September and (d) 17 December 2017. The corresponding vertical cross sections of shear at 30° W is shown in lower panel (e-h). The solid black line represent the 3.5 PVU as a dynamical tropopause, grey lines represent the potential temperature starting from 280 K (bottom) to 380 K (top) with 10 K increments, thick green lines show the horizontal wind speed (30, 45, 60 $\mathrm{m\,s^{-1}}$) and cloud ice water content with blue lines ($5 \times 10^{-6}$, $10 \times 10^{-6}$ kg kg$^{-1}$).

disturbances on larger scales and GW on smaller scales being a key contributor to the high shear abundance in this region. Moreover, such pronounced shear is often linked to tropopause disturbances and has been observed on the order of $10^{-2}$–$10^{-3}\,\mathrm{s^{-1}}$ (Lane et al., 2004; Kaluza et al., 2021), occurring particularly in dynamically active regions such as jet streaks and frontal zones (Koch et al., 2005; Wang and Zhang, 2007). The enhanced shear is evident in the ridge of the baroclinic wave, as well as observed partly above a region of ice cloud occurrence (Fig. 9e, h). This region is strongly affected by a small-scale wave pattern related to propagating inertia GWs which is evident in the isolines of potential temperature and PV. As discussed above, these small-scale GWs are one source of the enhanced values of shear. Another source could be radiative cooling below and at the tropopause related to ice clouds or moist dynamics related to the upper tropospheric region. However, the mechanism behind the shear generation is discussed in Umbarkar and Kunkel (2025). They show that the latent heat release from the lower troposphere can amplify GWs, foster vertical motions, and thereby lead to enhanced shear generation in the upper troposphere and above in the LMS.

https://doi.org/10.5194/egusphere-2026-413
Preprint. Discussion started: 23 February 2026


Overall, the GWs alter the flow on small-scales which could lead to enhanced small-scale divergence and shear occurrence. Based on case studies, we can infer that the GWs that propagate upwards show a spatial and temporal co-location with vertical wind shear. Yet, the question remains whether we see a similar link on larger (spatial and temporal) scales.

### 4.2 Intra-monthly variability of zonal GW forcings and momentum fluxes

We now examine the GW activity in terms of zonal GW forcing and GW momentum fluxes across our analysis year in greater detail.

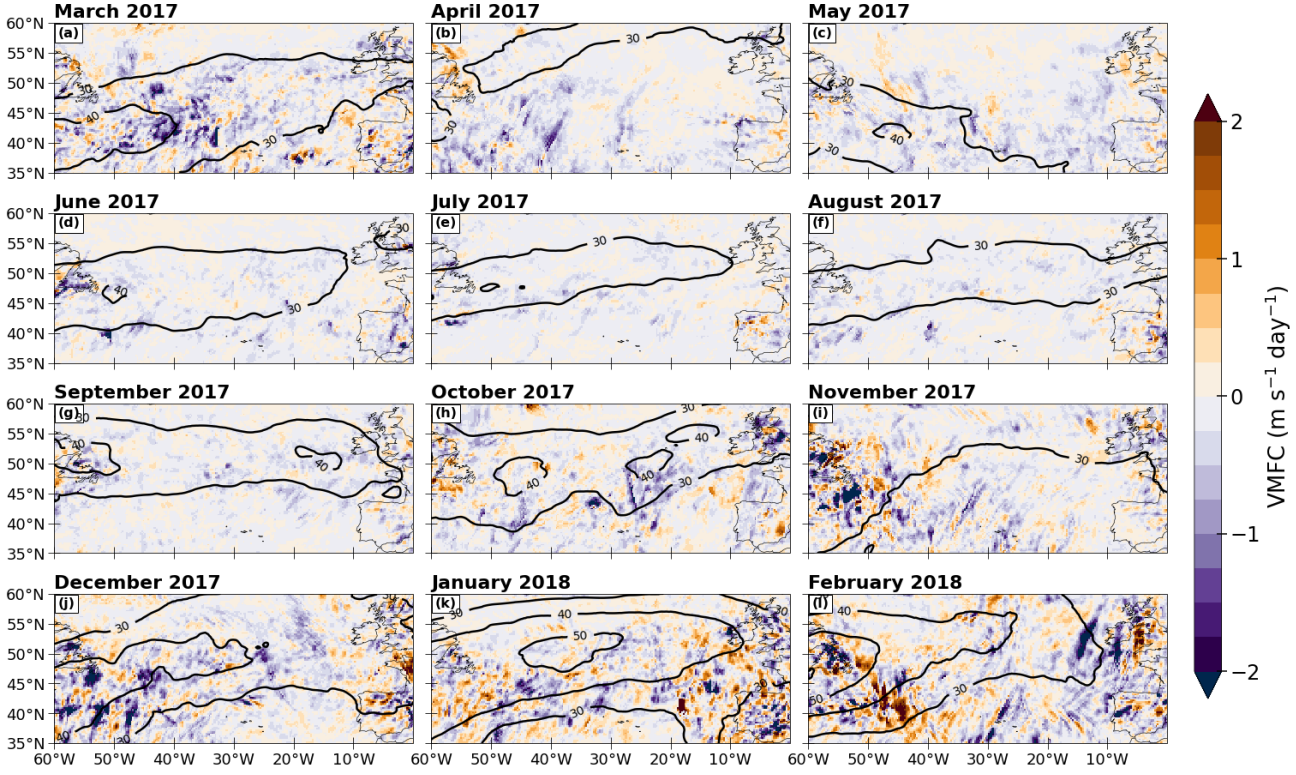


**Figure 10.** Monthly distribution of VMFC (in $\mathrm{m\,s^{-1}\,day^{-1}}$) between dynamical tropopause and 1.5 km above in the North Atlantic from March 2017 to February 2018. The solid black lines represents the horizontal wind beginning at 30 m s$^{-1}$ in steps of 10 m s$^{-1}$ at 11 km altitude.

Figure 10 shows the monthly mean distribution of GW related VMFC between the dynamical tropopause and 1.5 km above the tropopause height in NA. In general, the VMFC distribution is not zonally uniform, but rather with maxima concentrated along the jet stream region and minima over the subtropical Atlantic. Additionally, the monthly mean VMFC patterns reveal a pronounced seasonal variability. The dominance of GWs occur during winter (December–February; Fig. 10j-l) over the eastern NA, potentially as a result of the flow over Appalachian mountains, while weaker magnitudes are found during summer (June–August).

https://doi.org/10.5194/egusphere-2026-413
Preprint. Discussion started: 23 February 2026


The spatial distribution of VMFC can be related to distinct GW source mechanisms that vary seasonally. During winter months, the enhanced fluxes over the northeastern American continent and adjacent ocean are likely driven by strong surface winds and/or orographic forcing along steep terrain. In contrast, during summer, the weaker and patchier GW activity around 20–30° W and near the Iberian Peninsula (Fig. 10e) likely reflects orographic generation of GWs in association with strong surface winds such as katabatic winds (Watanabe et al., 2006). Similar localized enhancements also appear in June and September, suggesting intermittent wave propagation under favorable synoptic conditions.

From a dynamical perspective, the sign and structure of VMFC provide the direction of GW momentum transfer. According to linear wave theory, the direction of the horizontal momentum flux vector is the same as that of wavenumber vector of GWs if they propagate energy upward. In the LMS, VMFC is predominantly negative, particularly near the jet streak region, indicating that upward-propagating GWs deposit westward momentum. This spatial correspondence between enhanced negative fluxes and the jet region suggests that GWs generated upstream contribute to momentum deposition far from their source, modulating the local mean flow.

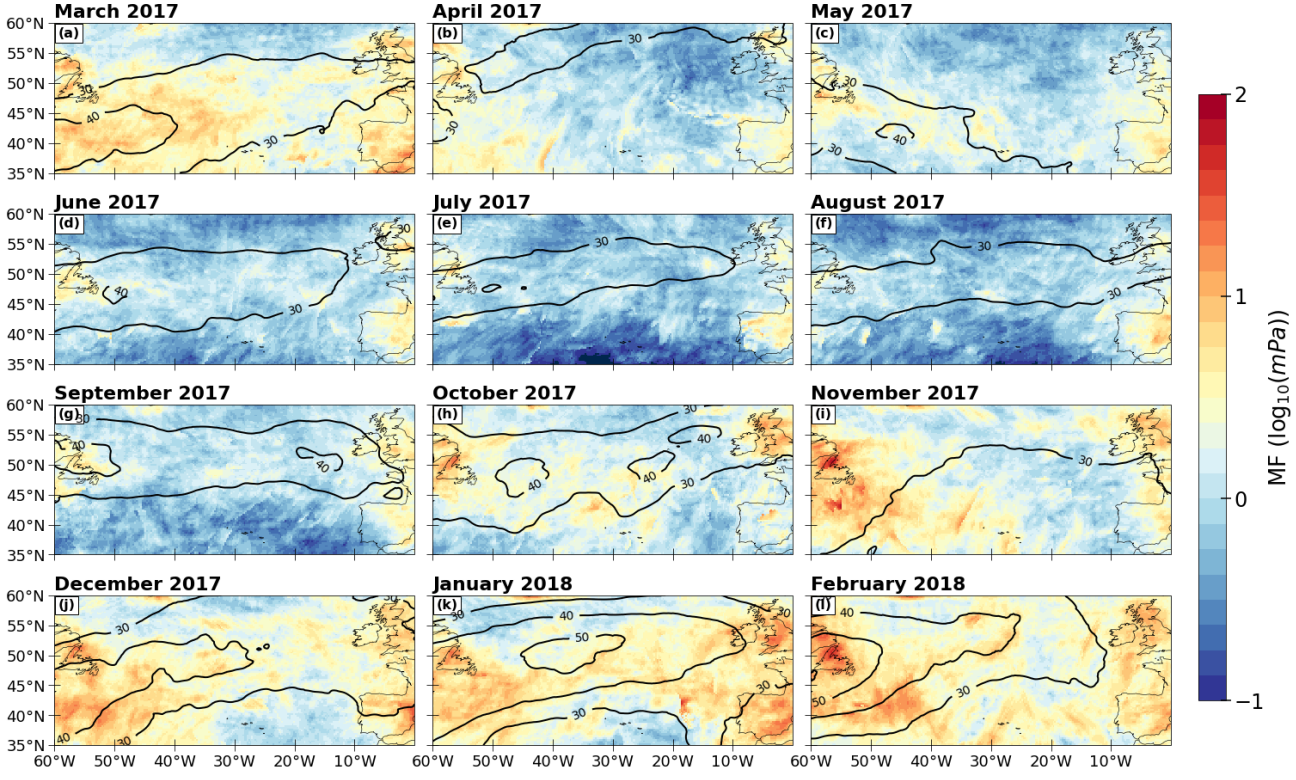


**Figure 11.** Monthly mean distribution of absolute GW momentum flux (in $\log_{10}(\mathrm{mPa})$) between dynamical tropopause and 1.5 km above in the North Atlantic from March 2017 to February 2018. The solid black lines represents the horizontal wind beginning at 30 m $s^{-1}$ in steps of 10 m $s^{-1}$ at 11 km altitude.

https://doi.org/10.5194/egusphere-2026-413
Preprint. Discussion started: 23 February 2026


The corresponding monthly mean distribution of GW momentum flux between the dynamical tropopause and 1.5 km above it (Fig. 11) reveal similar spatial patterns to those seen in momentum flux convergence, with the largest magnitudes co-located with the subtropical and polar-front jet regions. Enhanced MF values exceeding 1.5 $\log_{10}(\mathrm{mPa})$ are concentrated over the western and central NA, particularly along the jet exit regions and baroclinic zones. The spatial structure of the winter maxima suggests that GWs are generated predominantly in regions of strong flow over steep orography and near the exit regions of upper-level jets. Secondary MF enhancements over the oceanic regions east of North America imply efficient propagation of waves generated upstream, as well as additional sources linked to jet streak dynamics and frontogenesis. In contrast, weaker magnitudes occur in summer in the equatorward and downstream regions, when large-scale baroclinicity and jet intensity are reduced.

Overall, the observed transition from localized summer maxima to broad winter enhancements reflects the seasonal strengthening and poleward displacement of the upper-tropospheric jet system, which governs both the generation and vertical propagation of GWs. This emphasizes the dominant role of large-scale jet dynamics and orographic forcing in shaping the spatial and temporal variability of GW-driven momentum transport over the NA. Moreover, the vertical momentum flux convergence provides a peak GW forcing up to -2 $\mathrm{ms^{-1}day^{-1}}$ around 40–50° N are the regions of pronounced shear. Altogether, the regions of strong shear identified earlier shows a spatiotemporal co-location with intense GW activity also on a larger spatial and temporal scales, suggests that GWs contribute to conditions that favor enhanced shear encounters. In addition, momentum deposition associated with GW breaking could further intensify this shear generation.

This further motivates a deeper look at the significance of small–scale GWs to high vertical shear, and subsequently to the potential turbulence occurrence in the LMS. In the following, we therefore shift our discussion to the occurrence of dynamic instability associated with GWs and GW-induced shear over the North Atlantic.

### 4.3 Analysis of turbulence diagnostics in the LMS

#### 4.3.1 Dynamic instability

On small scales in time and space, there exists a strong co-location between GW and enhanced vertical shear in the lower stratosphere (see Sect. 3 and Sect. 4.2). Before we discuss the GW-induced shear instabilities, we first look deeper into the occurrence of dynamic instability in the LMS by assessing the relation between static stability, vertical shear and low Richardson-numbers. Regions with enhanced potential for turbulence are identified using a threshold of $0 \leq Ri \leq 1$, following previous studies (e.g., Lane et al., 2003; Olsen et al., 2013; Wang and Fu, 2021; Kaluza et al., 2021) and considering resolution-dependent effects (e.g., Shao et al., 2023), thereby capturing the most dynamically unstable and potential turbulent regions. The LMS is defined here as the region between the 3.5 PVU dynamical tropopause (lower boundary) and 380 K isentropic level (upper boundary). The upper boundary corresponds to the height of the tropical lapse rate tropopause (e.g., Holton et al., 1995; Weyland et al., 2025). Note that for this analysis, only data points found in the LMS are taken into account.

We start with the distribution of occurrence frequencies of squared Brunt-Vaisälä frequency $N^2$ and the vertical shear $S^2$ in the LMS over the NA, shown in the form of two-dimensional probability density function (PDF) as monthly distributions from

https://doi.org/10.5194/egusphere-2026-413
Preprint. Discussion started: 23 February 2026


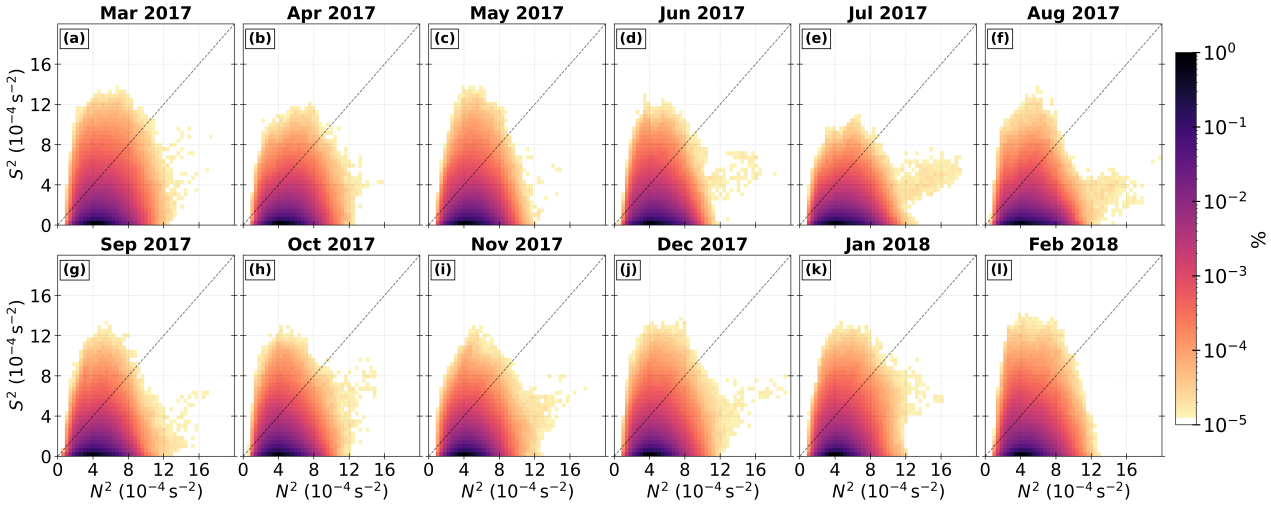


**Figure 12.** Relative occurrence frequency distribution of $N^2$-$S^2$ pairs in the LMS from March 2017 to February 2018. The occurrence frequencies are shown with logarithmic frequency contours. The black dashed line represent the $Ri$=1.

March 2017 to February 2018 (Fig. 12). The distributions reveal that the majority of occurrences are concentrated in regimes where $N^2$ exceeds $S^2$. This dominance of $N^2$ reflects the presence of the tropopause inversion layer (TIL), a sharp layer of enhanced stability just above the thermal tropopause (Birner, 2006). The TIL acts as a convectively stable region that inhibits vertical mixing and support the persistence of strong potential vorticity gradients across the tropopause (Kunkel et al., 2019). In contrast, the tail of the distribution extending toward larger $S^2$ marks higher likelihood of turbulence occurrence, i.e., dynamically active LMS, when the gradient Richardson number falls below 1. These $Ri \leq 1$ are most frequent during boreal winter and early spring, coinciding with strong jet activity and enhanced GW occurrence, and hence to the GW-mean flow interactions. This suggests that GWs, by locally amplifying vertical shear or reducing static stability, can contribute to transient instabilities in the lower stratosphere.

Furthermore, the seasonal modulation of $N^2$-$S^2$ distribution in LMS indicates a robust year-round strong shear signature, with strongest occurrences in winter and spring. The enhanced shear and reduced $Ri$ during winter imply a stronger potential for dynamic instability occurrence and a higher likelihood of shear-induced turbulent mixing, whereas summer months are dominated by a more stable TIL signature with reduced GW influence.

It is important to note that higher shear alone does not translate into the occurrence of turbulence and mixing. Related to that, the next step is to assess whether turbulence also occurs in the region of enhanced shear occurrences. Since turbulence is a rare event under general atmospheric conditions (Sharman et al., 2012; Dörnbrack et al., 2022), even in the LMS, we expect only a few data points to exhibit potential for dynamic instability. This becomes evident when joint PDFs of $N^2$ and $S^2$ reveal an indication of the occurrence of potential turbulence in the LMS with respect to $Ri$ (Fig. 12). Here we observe substantial values of $S^2$ maximum which are attributed to low $Ri$. This is further supported by the relative distribution of Richardson numbers

https://doi.org/10.5194/egusphere-2026-413
Preprint. Discussion started: 23 February 2026


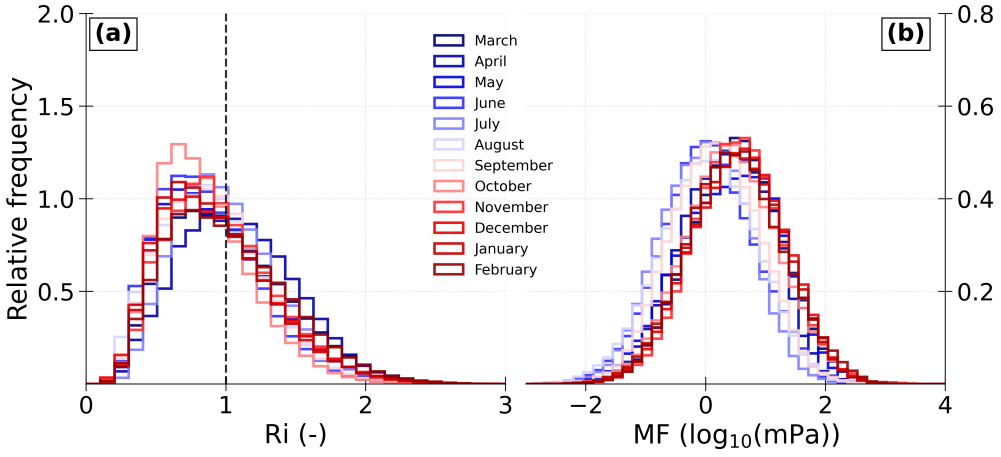


**Figure 13.** Relative occurrence frequency distribution of (a) $Ri$ that is associated with $S^2 \geq S_t^2$ and (b) the logarithm of absolute momentum flux conditioned on $S^2 \geq S_t^2$ associated with $0 \leq Ri \leq 1$ displayed in panel (a) in the LMS from March 2017 (blue) to February 2018 (red). The black dashed line in (a) represent the $Ri$=1.

that corresponds to the region of $S^2 \geq S_t^2$ (Fig. 13a). The large proportion of grid volumes that exceeds $S_t^2$ are located above the $Ri$=1 isoline, which constitutes the greater part of $Ri \leq 1$ within the LMS.

The distribution peaks at $Ri$=0.7 are mostly associated with vertical wind shear $S^2 \geq 4 \times 10^{-4}\,\mathrm{s}^{-2}$ and span over a broad spectrum of larger Richardson numbers of value up to 2 in the LMS. This further agrees with the Kaluza et al. (2021), suggesting that LMS is mostly dynamically unstable in the presence of strong vertical wind shear. In addition, the question remains whether these strong shear occurrences in the vicinity of low $Ri$ are attributed to GWs. The occurrence of MF in the vicinity of $S^2 \geq S_t^2$ that is associated with $0 \leq Ri \leq 1$ (Fig. 13b) shows higher positive MF in winter and slightly less in summer months. This enhanced GW activity in terms of MF reveals that GWs, along with other small-scale features, contribute to at least part of the pronounced shear that causes potential turbulence occurrence in the LMS. Yet, how much of the GWs contribute to shear and turbulence generation in the LMS remains unclear. This will be briefly addressed in the following section.

#### 4.3.2 GWs, shear and shear perturbations prone to potential turbulence: Coincidental or correlated?

At this point, the results obtained from the wind shear and mean state of GW fields could be questioned: what if the shear and small-scale features concerned, for instance GWs, are only tied to the synoptic feature, such as flow imbalances, but not to the turbulence occurrence? That is a similar pattern will be obtained, if we randomly pick regions that show the co-location, regardless of whether the location is turbulent or not. The justification given above relies on the previous studies, but it can also be answered with the correlation between small-scale shear and GW fluxes or forcings.

One question which initiated this study is related to the contribution of GWs to shear generation in the LMS and their role in shaping the TSL. For this, we move our discussion towards the relation between GWs and shear, as well as GW-induced shear in the LMS. Initially, we want to discuss the relative contribution of small-scale shear to total shear. We focus on the monthly

https://doi.org/10.5194/egusphere-2026-413
Preprint. Discussion started: 23 February 2026


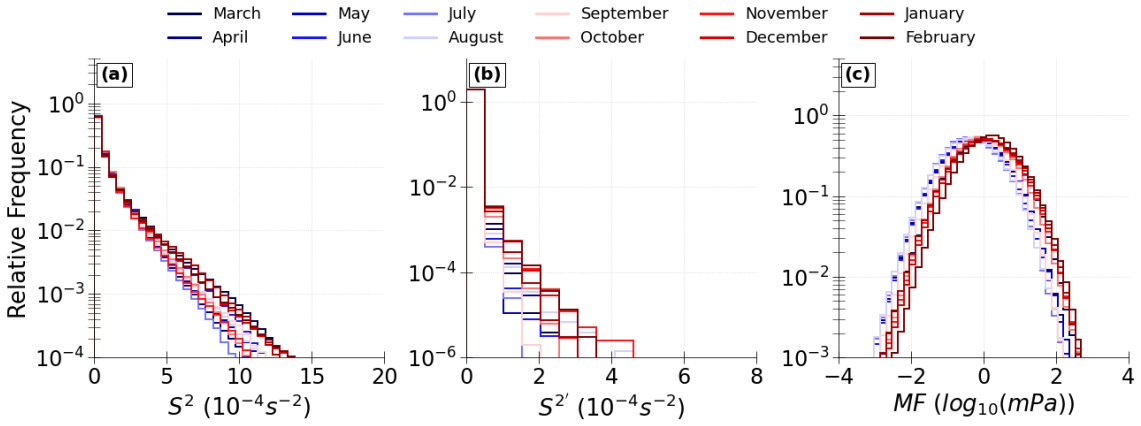


**Figure 14.** Relative frequency distribution of (a) $S^2$, (b) $S^{2'}$ and (c) the logarithm of absolute GW momentum flux over the LMS from March 2017 to February 2018.

occurrence of shear $S^2$, shear due to small-scale dynamics $S^{2'}$ and the momentum flux MF in the LMS (see Fig. 14). Both large-scale and small-scale shear indicate that the largest shear values are rare events; however, as noted before, the largest shear values occur during the winter months. During the summer months, the largest shear values have lesser occurrences. As expected based on its derivation, the occurrence frequencies of $S^{2'}$ are much smaller than those of $S^2$. We note again that we regard $S^{2'}$ as a proxy for the behavior of the smallest scales which are resolved by ERA5 and to estimate whether these small-scales behave differently than the large-scales. The distribution of MF (Fig. 14c) shows temporal variation in the higher occurrences of the distribution, where the distinct separation between the higher MF occurrences are evident in September to February (autumn and winter) months and the relatively lower occurrences in March to August (spring and summer) months. There is an increase in the occurrence of $S^2$ maxima, particularly during the intense GW activity. Under the assumption that $S^2$ is strongly under the influence of GW activity, this, in turn, suggests a substantial contribution of GWs to the generation of the largest shear values.

We will further explore the relation between small-scale shear and momentum flux in greater detail through the joint PDFs (Fig. 15). If GWs contribute to the generation of shear and turbulence in the LMS, a positive correlation between $S^{2'}$ and MF is expected in case of turbulence occurrence. The monthly distribution of data points of $S^{2'}$ and MF in the vicinity of $0 \leq Ri \leq 1$ indicate the positive correlation between these two quantities (Fig.15). The higher (lower) abundance of this relation is observed in the winter (summer) months. In all months, there is positive correlation in a sense that larger values of $S^{2'}$ occur preferentially during larger MF. Notably, the distribution of MF is mostly shifted toward larger values in the proximity of potential turbulence, with maxima occurring on the order of $10^1$ to $10^3$ mPa, while the corresponding non-turbulent distribution of MF in Fig. 14c is more centered around 0. Interestingly, there is a higher positive correlation observed in November, which could stem from the intense GW activity, likely associated with baroclinic waves in the NA storm track region that is coming from the Atlantic Northeast (region of eastern North America). Overall, this can be interpreted as an indication that the small-

https://doi.org/10.5194/egusphere-2026-413
Preprint. Discussion started: 23 February 2026


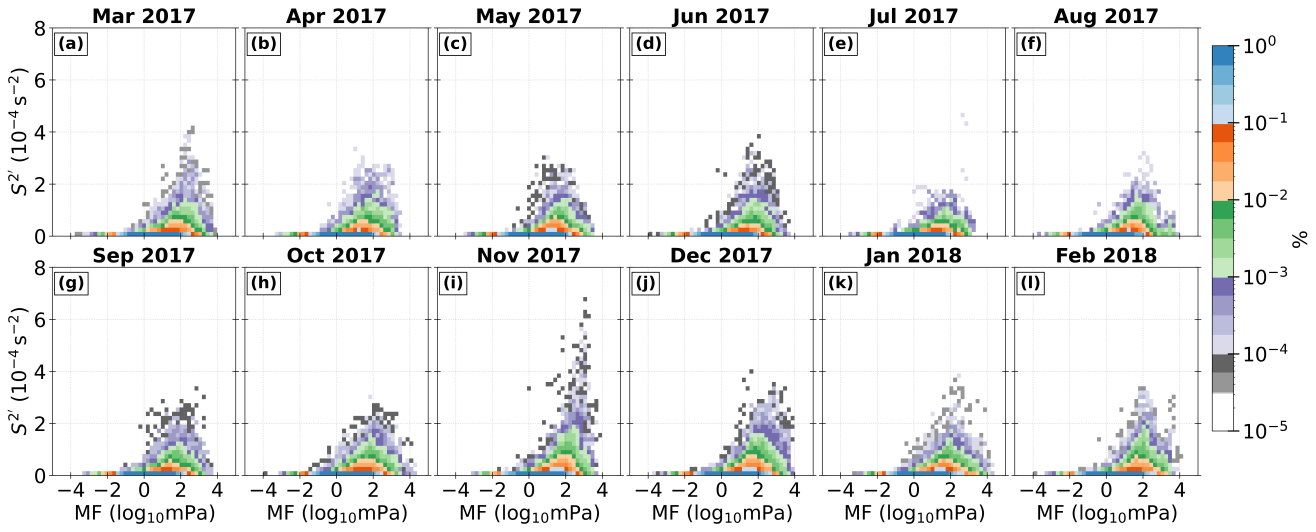


**Figure 15.** Relative occurrence frequency distribution of the logarithm of absolute momentum flux due to GWs-vertical shear perturbations pair in the LMS for $0 \leq Ri \leq 1$ over the North Atlantic LMS from March 2017 to February 2018. Normalized counts of PDFs distribution is shown. Logarithmic occurrence frequency color scale is applied.

scale processes–particularly the GWs–contribute substantially to the occurrence of strong shear perturbations and potential turbulence in the LMS.

It is important to note that the relation between total wind shear $S^2$ and MF in the vicinity of $0 \leq Ri \leq 1$ holds the slightly weak positive correlation, albeit an indication of the co-occurrences discussed in Fig. 14 in the paragraph above (refer also Fig. A1). This will be elaborated further in the following paragraph. Conversely, a strong positive correlation is noted between the shear perturbations and GW related MF under the potential turbulence occurring environment in LMS, which are associated with the dynamic instability conditions. Hence, the observed relationship between shear perturbations and intensity of GWs suggests that the GWs exhibit greater intensity during turbulent episodes.

Finally, we want to assess whether zonal GW forcing is related to the shear enhancement during the turbulent episodes or is merely a coincidence in the LMS. We explore this relation through the joint probability distribution of VMFC and vertical shear in the LMS in case of potential turbulence occurrence (Fig. 16). We anticipate higher co-occurrences of both parameters in the vicinity of turbulent region where momentum-flux convergence occurs, as upward-propagating GWs deposit their momentum in the subsequent region and thereby enhance local vertical wind gradients. This is confirmed in the PDFs: in all months, the distributions narrow toward larger shear and simultaneously shift toward more negative VMFC values (purple and green colors), results in a unimodal distribution which peaks around $\sim 12 \times 10^{-4}\,\mathrm{s}^{-2}$ vertical shear. Specifically, the distribution of VMFC, exceeding the range of $\pm 0.5\ \mathrm{m\,s^{-1}\,day^{-1}}$, broadens during winter months mainly with higher occurrences (see red colors), indicating that the strongest shear occurrences preferentially coincide with regions of enhanced upward momentum flux convergence. In contrast, this distribution is narrowest for summer months where profiles are rarely found outside the range

https://doi.org/10.5194/egusphere-2026-413
Preprint. Discussion started: 23 February 2026


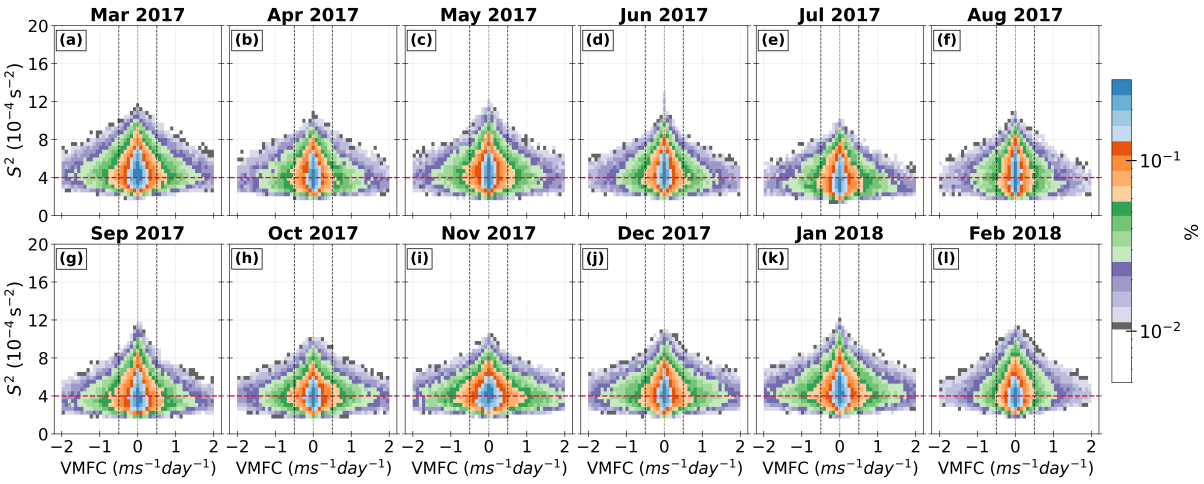


**Figure 16.** Relative occurrence frequency distribution of VMFC vs. vertical shear $S^2$ in the LMS for $0 \leq Ri \leq 1$ over the North Atlantic LMS from March 2017 to February 2018. Dashed red line indicate $S^2 = S_t^2$. Vertical dashed black lines mark the $\pm$ 0.5 range for readability.

of $\pm 0.5\ \mathrm{m\,s^{-1}\,day^{-1}}$. This coupling is most pronounced during winter, when baroclinic activity and jet strength peak, leading to both higher shear values and more intense GW forcing (see also discussion in Sect. 4.2). In summer, the relationship remains detectable but is rather weak and confined to lower shear values. Interestingly, the previously noted strong linkage between shear perturbations and MF in November is reaffirmed here: VMFC-$S^2$ PDFs show that the large GW zonal forcing aligns with the upper tail of the shear spectrum. This confirms that the intense shear observed during this month is not merely a product of jet imbalances but is mostly dynamically reinforced by active GW forcing linked to baroclinically unstable background flow. In conclusion, this relation provides compelling evidence that small-scale GWs play an active role in amplifying vertical wind shear in the LMS and contribute to the seasonal modulation of dynamical instability and turbulence susceptibility in the extratropical UTLS.

## 5 Summary

In this study we aimed to assess the role of resolved GWs in modulating the sharp gradients of vertical wind and shear layers near the extratropical tropopause. More specifically, we wanted to analyse the role gravity waves to the formation of vertical wind shear and associated turbulence in the lowermost stratosphere (LMS) over the North Atlantic (NA) using ECMWF ERA5 reanalysis data. There are several key points in this study which are important to highlight and discuss:

– First, we use the high-resolution ERA5 reanalysis which partially resolves the GW spectrum in the UTLS. This data set allowed us to analyse GWs, GW-induced shear, and the occurrence of the tropopause shear layer (TSL) over the North Atlantic domain. Our results demonstrate that there is a quasi-permanent layer of high shear occurrences just above the tropopause which has formerly been framed as the TSL (Kaluza et al., 2021). This TSL shows an annual cycle with

https://doi.org/10.5194/egusphere-2026-413
Preprint. Discussion started: 23 February 2026


maximum values during winter and minimum values during summer. The enhanced shear occurs in various regions and is related to specific processes related to large and small-scale dynamics, among others the occurrence of small-scale GWs associated with baroclinic waves in the extratropics.

- A similar analysis of GW momentum fluxes and turbulence diagnostics, in a tropopause-relative coordinate system, reveals the distinct seasonality of these parameters. More so, the analysis additionally shows that (i) enhanced GW momentum fluxes and strong vertical shear occur in the same regions in the vertical on a monthly basis, and (ii) all turbulence indices exhibit maxima both in the upper troposphere, and in the LMS, thus partially overlapping with the regions of enhanced vertical shear in the vicinity of intense GW activity.

- Furthermore, the TSL is located near regions of pronounced GW momentum flux above the extratropical tropopause. As such, the TSL may be regarded as a key indicator for nonlinear wave-mean-flow interaction and, consequently, of momentum deposition (Zhang et al., 2019; Bense, 2019; Kaluza et al., 2021). After detailed inspection of vertical profiles of the wind shear and TI1/TI2, it is revealed that these (clear-air) turbulent layers are generated at least partly by small-scale GW-induced shear above a tropospheric jet.

Overall this analysis presents a step towards a better understanding of GW-scale processes influencing and/or contributing to the dynamical structure of the transition region between the troposphere and the stratosphere, and above, i.e., the LMS in the extratropics. The GWs processes can have several implications in the LMS:

- GWs in the LMS are predominantly concentrated along the flanks of the upper-tropospheric jet, with a pronounced seasonal cycle. GW fluxes and associated shear are strongest in winter and weakest in summer, consistent with previous climatological analyses (e.g., Kaluza et al., 2021). This seasonality reflects enhanced baroclinic activity and GW generation during winter, with stronger vertical propagation from the upper troposphere into the lowermost stratosphere and above.

- The relative contribution of GWs to shear generation is found to be notable, especially in the winter in the lower stratosphere, where the convergence of vertical momentum provides a peak forcing of up to -2 $\mathrm{m\,s^{-1}\,day^{-1}}$ in the mid-latitude between 45–55° N. The strong vertical gradients in static stability near the tropopause make the UTLS particularly sensitive to GW forcing. The estimated peak momentum flux associated with the most intense shear and turbulence is on the order of $\sim 10^2$ mPa. This also reveals the presence of moderate upward propagating GWs through the LMS, producing vertical shear of $\sim 10^{-4}\,\mathrm{s^{-2}}$ magnitude, thereby triggering local instabilities.

- Regions of enhanced GW momentum flux converge with zones of intensified vertical shear, particularly in the vicinity of the tropopause. A clear positive correlation is found between GW-induced shear and absolute GW momentum flux, indicating that small-scale GWs are closely linked to the occurrence of dynamically unstable shear layers. This suggests that GWs act as an important mechanism in the formation of shear layers in the LMS, which in turn contribute to the conditions conducive for clear-air turbulence generation.

https://doi.org/10.5194/egusphere-2026-413
Preprint. Discussion started: 23 February 2026


In summary, the high-resolution ERA5 reanalysis forms a natural bridge between observations and free running climate models, and the outcomes presented herein offer new insights into the cascade of GW-driven processes within the extratropical UTLS, with the need for prediction of clear-air turbulence which is a major concern in aviation safety. Moreover, the ERA5 reanalysis data at least partially resolves GWs, allowing for an evaluation of small-scale GWs contribution to the climatological tropopause shear layer. Ultimately, the quasi-climatological distribution of GW activity and associated shear highlights that GW specifically play an important role in the formation and maintenance of the TSL. More generally, this can have larger implications for the dynamics and the composition in the ExTL. The latter is related to mixing layer around the extratropical tropopause which is, however, beyond the scope of current analysis.

Apart from the GWs contribution to shear, many questions remain about the GW momentum fluxes and their probability distributions, some of which could be addressed by further analysis on large eddy simulations of individual events in different geographical regions. Relating the momentum fluxes to the phase speeds could also provide a more direct interpretation on a relationship that is commonly used in the parameterizations (e.g., Alexander and Dunkerton, 1999). Moreover, the vertical shear based on GW propagation through the tropopause and lowermost stratosphere have been discussed so far (e.g., Fritts and Alexander, 2003; Kunkel et al., 2019; Kaluza et al., 2021; Umbarkar and Kunkel, 2025; Umbarkar et al., 2025), yet the effect of GW dissipation on the shear instability remains to be understood. Also, intermittency of GW must be taken into account when extrapolating regional turbulence occurrences to the global statistics in order to properly describe the systems. More case studies based on the in-situ observations as well as the climatological view like the one presented in this study might help to better understand the impact of GWs on the energy budget and the turbulent transport in the atmosphere.

*Data availability.* ERA5 model level data was retrieved from the MARS archive. The data is also publicly available from Copernicus Climate Change Service (C3S) Climate Data Store using the CDS API. The dataset used is: "ERA5: Fifth generation of ECMWF atmospheric reanalyses of the global climate" https://doi.org/10.24381/cds.143582cf (last access: 14 December 2025)

https://doi.org/10.5194/egusphere-2026-413
Preprint. Discussion started: 23 February 2026


## Appendix A: Method used to derive resolved GW momentum fluxes

For the calculations of GW perturbations from synoptic-scale structures we use a hybrid method (similar to Wei et al., 2022; Umbarkar and Kunkel, 2025; Zhang et al., 2025; Umbarkar et al., 2025) which applies a dynamical as well as statistical approach. We first divide the flow in its divergent and rotational component using a Helmholtz decomposition technique, i.e., the dynamical approach. Next, we apply a filter in spectral space using a one-dimensional zonal FFT over the entire northern hemisphere as part of the statistical approach. The further analysis is then performed only over the selective North Atlantic domain. With this additional spectral filter we remove the contributions from wavenumber 0 to 20, i.e.,

$$u' = u_{\text{div}} - (u_{\text{div}})_{k \leq 21} \tag{A1}$$

The retrieved part is the perturbation from synoptic-scale structures and is then denoted with primes ($'$). Note here that the sensitivity tests with wavenumber cutoff values of $\pm 4$ showed no significant variation in the resulting prime quantities. It should be noted that, since GW characteristics are latitude and height dependent, there is no universal constant cutoff that works globally (Procházková et al., 2023).

The overline showcasing the perturbation products (i.e. $\overline{u'w'}$ and $\overline{v'w'}$) are computed using a low-pass filtering of the quadratic quantities that uses the same Gaussian spectral filter as in Kruse and Smith (2015). This filtering is to ensure that the flux estimates are physically meaningful, as direct pointwise computation of these second-order terms without low-pass filtering or areal averaging would not appropriately capture the wave-induced momentum transport (see also Wei et al., 2022). We emphasize that our hybrid approach is well justified in the UTLS and follows the commonly used GW scale separation methods as in Zhang et al. (2025); Lehmann et al. (2012); Wei et al. (2016); Stephan et al. (2019); Strube et al. (2020); Gupta et al. (2021); Wei et al. (2022); Umbarkar and Kunkel (2025), despite different cutoff wavenumber used.

## Appendix B: Supporting information to Section 4.3.2

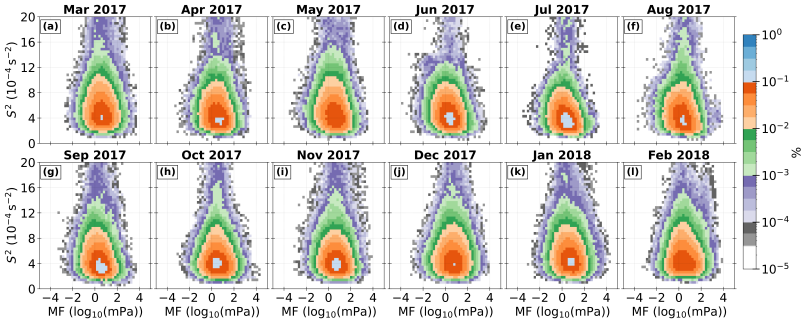


**Figure A1.** Relative occurrence frequency distribution of the logarithm of absolute momentum flux due to GWs and vertical shear pair in the LMS for $0 \leq Ri \leq 1$ over the North Atlantic LMS from March 2017 to February 2018. Normalized counts of PDFs distribution is shown. Logarithmic occurrence frequency color scale is applied.

https://doi.org/10.5194/egusphere-2026-413
Preprint. Discussion started: 23 February 2026


## Appendix B: Supporting information to Section 3.2

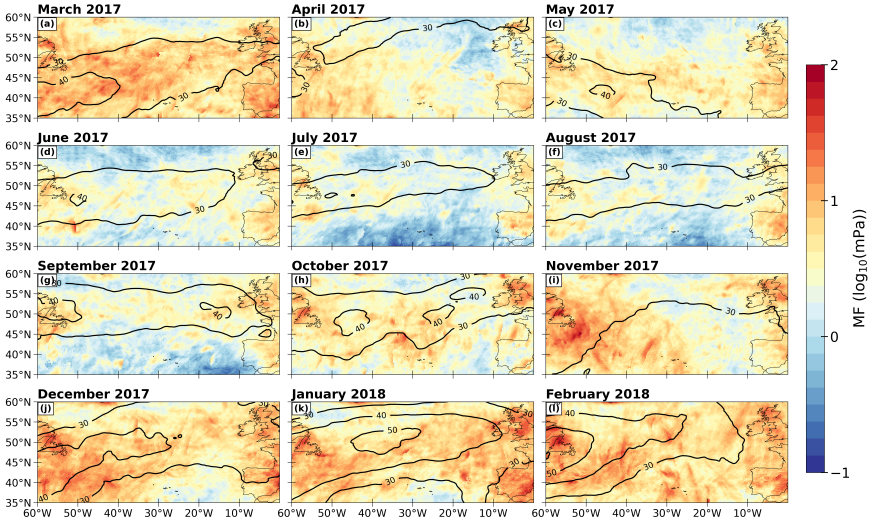


**Figure B1.** Monthly mean distribution of GW absolute momentum flux (MF, $\log_{10}(\mathrm{mPa})$) at dynamical tropopause altitude in the North Atlantic from March 2017 to February 2018.

## Appendix C: Supporting information to Section 4

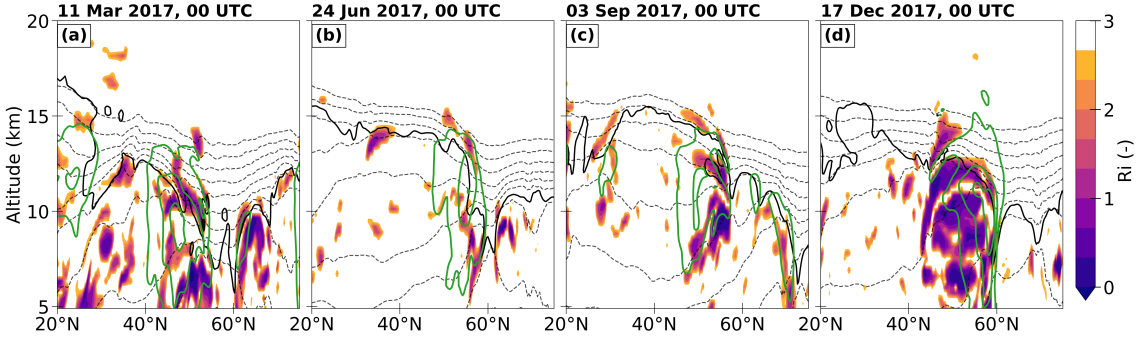


**Figure C1.** Vertical cross section of Gradient Richardson number at 30° W for (a) 11 March, (b) 23 June, (c) 3 September and (d) 17 December 2017. The solid black line represent the 3.5 PVU as a dynamical tropopause, grey lines represent the potential temperature starting from 280 K (bottom) to 380 K (top) with 10 K increments and thick green lines show the horizontal wind speed (30, 45, 60 $\mathrm{m\,s^{-1}}$).

https://doi.org/10.5194/egusphere-2026-413
Preprint. Discussion started: 23 February 2026


*Author contributions.* MU conceptualized the core research questions and goals with the help of DK. DK provided the data. MU conducted the data analysis, wrote the post-processing code, and drafted the paper. MU and DK jointly contributed to the interpretation of the results and edited the manuscript. UA commented on the manuscript. All authors contributed to the revised version of manuscript.

*Competing interests.* The authors declare that they have no conflict of interest.

*Acknowledgements.* This work was funded by the Deutsche Forschungsgemeinschaft (DFG, German Research Foundation)–TRR 301–Project-ID 428312742: “The tropopause region in a changing atmosphere, https://tpchange.de" sub-project B06. We greatly appreciate the feedback from Peter Hoor at an early stage of this study. Further thanks are due to Hans-Christoph Lachnitt from Johannes Gutenberg University Mainz and Pravin Punde from UiT The Arctic University of Norway, Tromsø, for their valuable comments and feedback on this work.

https://doi.org/10.5194/egusphere-2026-413
Preprint. Discussion started: 23 February 2026


## References

Achatz, U., Alexander, M. J., Becker, E., Chun, H.-Y., Dörnbrack, A., Holt, L., Plougonven, R., Polichtchouk, I., Sato, K., Sheshadri, A., Stephan, C. C., van Niekerk, A., and Wright, C. J.: Atmospheric Gravity Waves: Processes and Parameterization, Journal of the Atmospheric Sciences, 81, 237–262, https://doi.org/10.1175/jas-d-23-0210.1, 2024.

Alexander, M. J. and Dunkerton, T. J.: A Spectral Parameterization of Mean-Flow Forcing due to Breaking Gravity Waves, Journal of the Atmospheric Sciences, 56, 4167–4182, https://doi.org/10.1175/1520-0469(1999)056<4167:aspomf>2.0.co;2, 1999.

Alexander, M. J., Geller, M., McLandress, C., Polavarapu, S., Preusse, P., Sassi, F., Sato, K., Eckermann, S., Ern, M., Hertzog, A., Kawatani, Y., Pulido, M., Shaw, T. A., Sigmond, M., Vincent, R., and Watanabe, S.: Recent developments in gravity-wave effects in climate models and the global distribution of gravity-wave momentum flux from observations and models, Quarterly Journal of the Royal Meteorological Society, 136, 1103–1124, https://doi.org/10.1002/qj.637, 2010.

Banerjee, T., Borchert, S., Kim, Y.-H., Kosareva, A., Kunkel, D., Masur, G. T., Procházková, Z., Schmidli, J., Voelker, G. S., and Achatz, U.: The Impact of Non-Orographic Gravity Waves on Transport and Mixing: Effects of Oblique Propagation and Coupling to Turbulence, https://arxiv.org/abs/2508.20562, 2025.

Bense, V.: Modifikation von Schwerewellen bei Propagation durch die Tropopause - Idealisierte Modellstudien, Ph.D. thesis, https://doi.org/10.25358/OPENSCIENCE-2356, 2019.

Birner, T.: Fine-scale structure of the extratropical tropopause region, Journal of Geophysical Research Atmospheres, 111, 1–14, https://doi.org/10.1029/2005JD006301, 2006.

Chen, D., Strube, C., Ern, M., Preusse, P., and Riese, M.: Global analysis for periodic variations in gravity wave squared amplitudes and momentum fluxes in the middle atmosphere, Annales Geophysicae, 37, 487–506, https://doi.org/10.5194/angeo-37-487-2019, 2019.

de Medeiros, J. and Williams, P. D.: Future Trends in Upper-Atmospheric Shear Instability from Climate Change, Journal of the Atmospheric Sciences, 82, 2375–2392, https://doi.org/10.1175/jas-d-24-0283.1, 2025.

Dörnbrack, A., Bechtold, P., and Schumann, U.: High-Resolution Aircraft Observations of Turbulence and Waves in the Free Atmosphere and Comparison With Global Model Predictions, Journal of Geophysical Research: Atmospheres, 127, https://doi.org/10.1029/2022jd036654, 2022.

Dörnbrack, A., Lachnitt, H., Hoor, P., and Imazio, P. R.: Multiscale Dynamical Processes Shaping a Mixing Line, Journal of Geophysical Research: Atmospheres, 130, https://doi.org/10.1029/2025jd043527, 2025.

Drnbrack, A., Gerz, T., and Schumann, U.: Turbulent breaking of overturning gravity waves below a critical level, Applied Scientific Research, 54, 163–176, https://doi.org/10.1007/bf00849114, 1995.

Ellrod, G. P. and Knapp, D. I.: An Objective Clear-Air Turbulence Forecasting Technique: Verification and Operational Use, Weather and Forecasting, 7, 150–165, https://doi.org/10.1175/1520-0434(1992)007<0150:aocatf>2.0.co;2, 1992.

Fritts, D. C. and Alexander, M. J.: Gravity wave dynamics and effects in the middle atmosphere, Reviews of Geophysics, 41, https://doi.org/10.1029/2001rg000106, 2003.

Geller, M. A., Alexander, M. J., Love, P. T., Bacmeister, J., Ern, M., Hertzog, A., Manzini, E., Preusse, P., Sato, K., Scaife, A. A., and Zhou, T.: A Comparison between Gravity Wave Momentum Fluxes in Observations and Climate Models, Journal of Climate, 26, 6383–6405, https://doi.org/10.1175/jcli-d-12-00545.1, 2013.

https://doi.org/10.5194/egusphere-2026-413
Preprint. Discussion started: 23 February 2026


Gisinger, S., Wagner, J., and Witschas, B.: Airborne measurements and large-eddy simulations of small-scale gravity waves at the tropopause inversion layer over Scandinavia, Atmospheric Chemistry and Physics, 20, 10 091–10 109, https://doi.org/10.5194/acp-20-10091-2020, 2020.

Gultepe, I., Sharman, R., Williams, P. D., Zhou, B., Ellrod, G., Minnis, P., Trier, S., Griffin, S., Yum, S. S., Gharabaghi, B., Feltz, W., Temimi, M., Pu, Z., Storer, L. N., Kneringer, P., Weston, M. J., Chuang, H.-y., Thobois, L., Dimri, A. P., Dietz, S. J., França, G. B., Almeida, M. V., and Neto, F. L. A.: A Review of High Impact Weather for Aviation Meteorology, Pure and Applied Geophysics, 176, 1869–1921, https://doi.org/10.1007/s00024-019-02168-6, 2019.

Gupta, A., Birner, T., Dörnbrack, A., and Polichtchouk, I.: Importance of Gravity Wave Forcing for Springtime Southern Polar Vortex Breakdown as Revealed by ERA5, Geophysical Research Letters, 48, https://doi.org/10.1029/2021gl092762, 2021.

Gupta, A., Sheshadri, A., Alexander, M. J., and Birner, T.: Insights on Lateral Gravity Wave Propagation in the Extratropical Stratosphere From 44 Years of ERA5 Data, Geophysical Research Letters, 51, https://doi.org/10.1029/2024gl108541, 2024.

Hegglin, M. I., Boone, C. D., Manney, G. L., and Walker, K. A.: A global view of the extratropical tropopause transition layer from Atmospheric Chemistry Experiment Fourier Transform Spectrometer O3, H2O, and CO, Journal of Geophysical Research: Atmospheres, 114, https://doi.org/10.1029/2008jd009984, 2009.

Hersbach, H., Bell, B., Berrisford, P., Hirahara, S., Horányi, A., Muñoz-Sabater, J., Nicolas, J., Peubey, C., Radu, R., Schepers, D., Simmons, A., Soci, C., Abdalla, S., Abellan, X., Balsamo, G., Bechtold, P., Biavati, G., Bidlot, J., Bonavita, M., De Chiara, G., Dahlgren, P., Dee, D., Diamantakis, M., Dragani, R., Flemming, J., Forbes, R., Fuentes, M., Geer, A., Haimberger, L., Healy, S., Hogan, R. J., Hólm, E., Janisková, M., Keeley, S., Laloyaux, P., Lopez, P., Lupu, C., Radnoti, G., de Rosnay, P., Rozum, I., Vamborg, F., Villaume, S., and Thépaut, J.: The ERA5 global reanalysis, Quarterly Journal of the Royal Meteorological Society, 146, 1999–2049, https://doi.org/10.1002/qj.3803, 2020.

Hoffmann, L., Günther, G., Li, D., Stein, O., Wu, X., Griessbach, S., Heng, Y., Konopka, P., Müller, R., Vogel, B., and Wright, J. S.: From ERA-Interim to ERA5: the considerable impact of ECMWF's next-generation reanalysis on Lagrangian transport simulations, Atmospheric Chemistry and Physics, 19, 3097–3124, https://doi.org/10.5194/acp-19-3097-2019, 2019.

Holton, J. R., Haynes, P. H., McIntyre, M. E., Douglass, A. R., Rood, R. B., and Pfister, L.: Stratosphere-troposphere exchange, Reviews of Geophysics, 33, 403–439, https://doi.org/10.1029/95rg02097, 1995.

Hoor, P., Gurk, C., Brunner, D., Hegglin, M. I., Wernli, H., and Fischer, H.: Seasonality and extent of extratropical TST derived from in-situ CO measurements during SPURT, Atmospheric Chemistry and Physics, 4, 1427–1442, https://doi.org/10.5194/acp-4-1427-2004, 2004.

Jewtoukoff, V., Hertzog, A., Plougonven, R., Cámara, A. d. l., and Lott, F.: Comparison of Gravity Waves in the Southern Hemisphere Derived from Balloon Observations and the ECMWF Analyses, Journal of the Atmospheric Sciences, 72, 3449–3468, https://doi.org/10.1175/jas-d-14-0324.1, 2015.

Kaluza, T., Kunkel, D., and Hoor, P.: Composite analysis of the tropopause inversion layer in extratropical baroclinic waves, Atmospheric Chemistry and Physics, 19, 6621–6636, https://doi.org/10.5194/acp-19-6621-2019, 2019.

Kaluza, T., Kunkel, D., and Hoor, P.: On the occurrence of strong vertical wind shear in the tropopause region: a 10-year ERA5 northern hemispheric study, Weather and Climate Dynamics, 2, 631–651, https://doi.org/10.5194/wcd-2-631-2021, 2021.

Kaluza, T., Kunkel, D., and Hoor, P.: Analysis of Turbulence Reports and ERA5 Turbulence Diagnostics in a Tropopause-Based Vertical Framework, Geophysical Research Letters, 49, https://doi.org/10.1029/2022gl100036, 2022.

Kim, J.-H. and Chun, H.-Y.: Statistics and Possible Sources of Aviation Turbulence over South Korea, Journal of Applied Meteorology and Climatology, 50, 311–324, https://doi.org/10.1175/2010jamc2492.1, 2011.

https://doi.org/10.5194/egusphere-2026-413
Preprint. Discussion started: 23 February 2026


Kim, J.-H., Sharman, R., Strahan, M., Scheck, J. W., Bartholomew, C., Cheung, J. C. H., Buchanan, P., and Gait, N.: Improvements in Nonconvective Aviation Turbulence Prediction for the World Area Forecast System, Bulletin of the American Meteorological Society, 99, 2295–2311, https://doi.org/10.1175/bams-d-17-0117.1, 2018.

Kim, Y., Eckermann, S. D., and Chun, H.: An overview of the past, present and future of gravity-wave drag parametrization for numerical climate and weather prediction models, Atmosphere-Ocean, 41, 65–98, https://doi.org/10.3137/ao.410105, 2003.

Knox, J. A., McCann, D. W., and Williams, P. D.: Application of the Lighthill–Ford Theory of Spontaneous Imbalance to Clear-Air Turbulence Forecasting, Journal of the Atmospheric Sciences, 65, 3292–3304, https://doi.org/10.1175/2008jas2477.1, 2008.

Koch, S. E., Jamison, B. D., Lu, C., Smith, T. L., Tollerud, E. I., Girz, C., Wang, N., Lane, T. P., Shapiro, M. A., Parrish, D. D., and Cooper, O. R.: Turbulence and Gravity Waves within an Upper-Level Front, Journal of the Atmospheric Sciences, 62, 3885–3908, https://doi.org/10.1175/jas3574.1, 2005.

Kruse, C. G. and Smith, R. B.: Gravity Wave Diagnostics and Characteristics in Mesoscale Fields, Journal of the Atmospheric Sciences, 72, 4372–4392, https://doi.org/10.1175/jas-d-15-0079.1, 2015.

Kunkel, D., Hoor, P., Kaluza, T., Ungermann, J., Kluschat, B., Giez, A., Lachnitt, H.-C., Kaufmann, M., and Riese, M.: Evidence of small-scale quasi-isentropic mixing in ridges of extratropical baroclinic waves, Atmospheric Chemistry and Physics, 19, 12 607–12 630, https://doi.org/10.5194/acp-19-12607-2019, 2019.

Lachnitt, H.-C., Hoor, P., Kunkel, D., Bramberger, M., Dörnbrack, A., Müller, S., Reutter, P., Giez, A., Kaluza, T., and Rapp, M.: Gravity-wave-induced cross-isentropic mixing: a DEEPWAVE case study, Atmospheric Chemistry and Physics, 23, 355–373, https://doi.org/10.5194/acp-23-355-2023, 2023.

Lane, T. P., Sharman, R. D., Clark, T. L., and Hsu, H.-M.: An Investigation of Turbulence Generation Mechanisms above Deep Convection, Journal of the Atmospheric Sciences, 60, 1297–1321, https://doi.org/10.1175/1520-0469(2003)60<1297:aiotgm>2.0.co;2, 2003.

Lane, T. P., Doyle, J. D., Plougonven, R., Shapiro, M. A., and Sharman, R. D.: Observations and Numerical Simulations of Inertia–Gravity Waves and Shearing Instabilities in the Vicinity of a Jet Stream, Journal of the Atmospheric Sciences, 61, 2692–2706, https://doi.org/10.1175/jas3305.1, 2004.

Lee, D.-B., Chun, H.-Y., and Kim, J.-H.: Evaluation of Multimodel-Based Ensemble Forecasts for Clear-Air Turbulence, Weather and Forecasting, 35, 507–521, https://doi.org/10.1175/waf-d-19-0155.1, 2020.

Lee, J. H., Kim, J., Sharman, R. D., Kim, J., and Son, S.: Climatology of Clear-Air Turbulence in Upper Troposphere and Lower Stratosphere in the Northern Hemisphere Using ERA5 Reanalysis Data, Journal of Geophysical Research: Atmospheres, 128, https://doi.org/10.1029/2022jd037679, 2022.

Lehmann, C. I., Kim, Y.-H., Preusse, P., Chun, H.-Y., Ern, M., and Kim, S.-Y.: Consistency between Fourier transform and small-volume few-wave decomposition for spectral and spatial variability of gravity waves above a typhoon, Atmospheric Measurement Techniques, 5, 1637–1651, https://doi.org/10.5194/amt-5-1637-2012, 2012.

Lindzen, R. S.: Turbulence and stress owing to gravity wave and tidal breakdown, Journal of Geophysical Research: Oceans, 86, 9707–9714, https://doi.org/10.1029/jc086ic10p09707, 1981.

Luderer, G., Trentmann, J., Hungershöfer, K., Herzog, M., Fromm, M., and Andreae, M. O.: Small-scale mixing processes enhancing troposphere-to-stratosphere transport by pyro-cumulonimbus storms, Atmospheric Chemistry and Physics, 7, 5945–5957, https://doi.org/10.5194/acp-7-5945-2007, 2007.

Olsen, M. A., Douglass, A. R., and Kaplan, T. B.: Variability of extratropical ozone stratosphere–troposphere exchange using microwave limb sounder observations, Journal of Geophysical Research: Atmospheres, 118, 1090–1099, https://doi.org/10.1029/2012jd018465, 2013.

https://doi.org/10.5194/egusphere-2026-413
Preprint. Discussion started: 23 February 2026


Pan, L. L., Konopka, P., and Browell, E. V.: Observations and model simulations of mixing near the extratropical tropopause, Journal of Geophysical Research: Atmospheres, 111, https://doi.org/10.1029/2005jd006480, 2006.

Plougonven, R. and Snyder, C.: Gravity waves excited by jets: Propagation versus generation, Geophysical Research Letters, 32, https://doi.org/10.1029/2005gl023730, 2005.

Podglajen, A., Hertzog, A., Plougonven, R., and Legras, B.: Lagrangian gravity wave spectra in the lower stratosphere of current (re)analyses, Atmospheric Chemistry and Physics, 20, 9331–9350, https://doi.org/10.5194/acp-20-9331-2020, 2020.

Procházková, Z., Kruse, C. G., Alexander, M. J., Hoffmann, L., Bacmeister, J. T., Holt, L., Wright, C., Sato, K., Gisinger, S., Ern, M., Geldenhuys, M., Preusse, P., and Šácha, P.: Sensitivity of Mountain Wave Drag Estimates on Separation Methods and Proposed Improvements, Journal of the Atmospheric Sciences, 80, 1661–1680, https://doi.org/10.1175/jas-d-22-0151.1, 2023.

Schäfler, A., Harvey, B., Methven, J., Doyle, J. D., Rahm, S., Reitebuch, O., Weiler, F., and Witschas, B.: Observation of Jet Stream Winds during NAWDEX and Characterization of Systematic Meteorological Analysis Errors, Monthly Weather Review, 148, 2889–2907, https://doi.org/10.1175/mwr-d-19-0229.1, 2020.

Shao, J., Zhang, J., Wang, W., Zhang, S., Yu, T., and Dong, W.: Occurrence frequency of subcritical Richardson numbers assessed by global high-resolution radiosonde and ERA5 reanalysis, Atmospheric Chemistry and Physics, 23, 12 589–12 607, https://doi.org/10.5194/acp-23-12589-2023, 2023.

Sharman, R., Tebaldi, C., Wiener, G., and Wolff, J.: An Integrated Approach to Mid- and Upper-Level Turbulence Forecasting, Weather and Forecasting, 21, 268–287, https://doi.org/10.1175/waf924.1, 2006.

Sharman, R. D. and Pearson, J. M.: Prediction of Energy Dissipation Rates for Aviation Turbulence. Part I: Forecasting Nonconvective Turbulence, Journal of Applied Meteorology and Climatology, 56, 317–337, https://doi.org/10.1175/jamc-d-16-0205.1, 2017.

Sharman, R. D., Trier, S. B., Lane, T. P., and Doyle, J. D.: Sources and dynamics of turbulence in the upper troposphere and lower stratosphere: A review, Geophysical Research Letters, 39, https://doi.org/10.1029/2012gl051996, 2012.

Shaw, T. A., Baldwin, M., Barnes, E. A., Caballero, R., Garfinkel, C. I., Hwang, Y.-T., Li, C., O'Gorman, P. A., Rivière, G., Simpson, I. R., and Voigt, A.: Storm track processes and the opposing influences of climate change, Nature Geoscience, 9, 656–664, https://doi.org/10.1038/ngeo2783, 2016.

Stephan, C. C., Strube, C., Klocke, D., Ern, M., Hoffmann, L., Preusse, P., and Schmidt, H.: Intercomparison of Gravity Waves in Global Convection-Permitting Models, Journal of the Atmospheric Sciences, 76, 2739–2759, https://doi.org/10.1175/jas-d-19-0040.1, 2019.

Strube, C., Ern, M., Preusse, P., and Riese, M.: Removing spurious inertial instability signals from gravity wave temperature perturbations using spectral filtering methods, Atmospheric Measurement Techniques, 13, 4927–4945, https://doi.org/10.5194/amt-13-4927-2020, 2020.

Sutherland, B. R., Achatz, U., Caulfield, C.-C. P., and Klymak, J. M.: Recent progress in modeling imbalance in the atmosphere and ocean, Phys. Rev. Fluids, 4, 010 501, 2019.

Thompson, C. F. and Schultz, D. M.: The Release of Inertial Instability Near an Idealized Zonal Jet, Geophysical Research Letters, 48, https://doi.org/10.1029/2021gl092649, 2021.

Umbarkar, M. and Kunkel, D.: Contribution of gravity waves to shear in the extratropical lowermost stratosphere: insights from idealized baroclinic life cycle experiments, Atmospheric Chemistry and Physics, 25, 10 159–10 182, https://doi.org/10.5194/acp-25-10159-2025, 2025.

Umbarkar, M., Kunkel, D., Miltenberger, A., Lachnitt, H.-C., Kaluza, T., Schwenk, C., and Hoor, P.: Evidence of gravity wave contribution to vertical shear and mixing in the lower stratosphere: a WISE case study, Atmospheric Chemistry and Physics, https://doi.org/10.5194/egusphere-2025-5142, preprint, 2025.

https://doi.org/10.5194/egusphere-2026-413
Preprint. Discussion started: 23 February 2026


Wang, M. and Fu, Q.: Stratosphere-Troposphere Exchange of Air Masses and Ozone Concentrations Based on Reanalyses and Observations, Journal of Geophysical Research: Atmospheres, 126, https://doi.org/10.1029/2021jd035159, 2021.

Wang, S. and Zhang, F.: Sensitivity of Mesoscale Gravity Waves to the Baroclinicity of Jet-Front Systems, Monthly Weather Review, 135, 670–688, https://doi.org/10.1175/mwr3314.1, 2007.

Watanabe, S., Sato, K., and Takahashi, M.: A general circulation model study of the orographic gravity waves over Antarctica excited by katabatic winds, Journal of Geophysical Research: Atmospheres, 111, https://doi.org/10.1029/2005jd006851, 2006.

Wei, J., Zhang, F., and Richter, J. H.: An Analysis of Gravity Wave Spectral Characteristics in Moist Baroclinic Jet–Front Systems, Journal of the Atmospheric Sciences, 73, 3133–3155, https://doi.org/10.1175/jas-d-15-0316.1, 2016.

Wei, J., Zhang, F., Richter, J. H., Alexander, M. J., and Sun, Y. Q.: Global Distributions of Tropospheric and Stratospheric Gravity Wave Momentum Fluxes Resolved by the 9-km ECMWF Experiments, Journal of the Atmospheric Sciences, 79, 2621–2644, https://doi.org/10.1175/jas-d-21-0173.1, 2022.

Weyland, F., Hoor, P., Kunkel, D., Birner, T., Plöger, F., and Turhal, K.: Long-term changes in the thermodynamic structure of the lowermost stratosphere inferred from reanalysis data, Atmospheric Chemistry and Physics, 25, 1227–1252, https://doi.org/10.5194/acp-25-1227-2025, 2025.

Wright, C. J. and Hindley, N. P.: How well do stratospheric reanalyses reproduce high-resolution satellite temperature measurements?, Atmospheric Chemistry and Physics, 18, 13 703–13 731, https://doi.org/10.5194/acp-18-13703-2018, 2018.

Zhang, F., Wei, J., Zhang, M., Bowman, K. P., Pan, L. L., Atlas, E., and Wofsy, S. C.: Aircraft measurements of gravity waves in the upper troposphere and lower stratosphere during the START08 field experiment, Atmospheric Chemistry and Physics, 15, 7667–7684, https://doi.org/10.5194/acp-15-7667-2015, 2015.

Zhang, W., Peng, J., Zhang, W., Wang, S., Li, Z., and Hanyan, W.: Sensitivity of Gravity Wave Momentum Flux Estimates on Separation Methods, Monthly Weather Review, 153, 1721–1742, https://doi.org/10.1175/mwr-d-24-0272.1, 2025.

Zhang, Y., Zhang, S., Huang, C., Huang, K., and Gong, Y.: The Tropopause Inversion Layer Interaction With the Inertial Gravity Wave Activities and Its Latitudinal Variability, Journal of Geophysical Research: Atmospheres, 124, 7512–7522, https://doi.org/10.1029/2019jd030309, 2019.